

ARTICLE

# Opposing functions for retromer and Rab11 in extracellular vesicle traffic at presynaptic terminals

Rylie B. Walsh, Erica C. Dresselhaus, Agata N. Becalska, Matthew J. Zunitz, Cassandra R. Blanchette, Amy L. Scalara, Tania Lemos, So Min Lee, Julia Apiki, ShiYu Wang, Berith Isaac, Anna Yeh, Kate Koles, and Avital A. Rodal

**Neuronal extracellular vesicles (EVs) play important roles in intercellular communication and pathogenic protein propagation in neurological disease. However, it remains unclear how cargoes are selectively packaged into neuronal EVs. Here, we show that loss of the endosomal retromer complex leads to accumulation of EV cargoes including amyloid precursor protein (APP), synaptotagmin-4 (Syt4), and neuroglian (Nrg) at *Drosophila* motor neuron presynaptic terminals, resulting in increased release of these cargoes in EVs. By systematically exploring known retromer-dependent trafficking mechanisms, we show that EV regulation is separable from several previously identified roles of neuronal retromer. Conversely, mutations in *rab11* and *rab4*, regulators of endosome-plasma membrane recycling, cause reduced EV cargo levels, and *rab11* suppresses cargo accumulation in retromer mutants. Thus, EV traffic reflects a balance between Rab4/Rab11 recycling and retromer-dependent removal from EV precursor compartments. Our data shed light on previous studies implicating Rab11 and retromer in competing pathways in Alzheimer’s disease, and suggest that misregulated EV traffic may be an underlying defect.**

## Introduction

Transmembrane proteins are routed from the plasma membrane through endolysosomal trafficking pathways that determine whether cargoes are degraded or recycled (Naslavsky and Caplan, 2018). Neuronal function and survival depend on sorting between these pathways, and aberrant endosomal trafficking is linked to many neurodegenerative diseases, including Alzheimer’s disease (AD; Winckler et al., 2018). One possible fate for endosomal cargo is incorporation into extracellular vesicles (EVs). EVs include exosomes (derived when multivesicular bodies [MVBs] fuse with the plasma membrane, releasing their intraluminal vesicles [ILVs] from the cell) and microvesicles (which bud directly from the plasma membrane; van Niel et al., 2018). EVs contain signaling proteins, lipids, and nucleic acids, and mediate communication between cell types in the nervous system (Holm et al., 2018). Neuronal EVs also function in both intercellular propagation and clearance of pathogenic proteins, including the A $\beta$  fragment of amyloid precursor protein (APP), a central player in AD (Arbo et al., 2020; Song et al., 2020). However, the mechanisms for EV sorting of APP and other neuronal cargoes are poorly understood, and are challenging to study in vivo at presynaptic terminals, which may be important sites of APP fragment release (Lazarov et al., 2002; Lundgren et al., 2014; Yu et al., 2018).

Retromer complex, composed of Vps35, Vps26, and Vps29, mediates endosomal cargo sorting into membrane tubules and

buds (Seaman, 2021). Retromer retrieves cargoes from endosomes to the Golgi and plasma membrane, controls endosome maturation, facilitates autophagy, and influences mitochondrial fusion and function (Chen et al., 2019). The role of retromer in endosome-derived EV traffic is less clear. While depletion of retromer leads to increased APP in EVs released from HEK293T cells (Sullivan et al., 2011), others have found decreased EV levels of Wnt3A upon loss of retromer from this same cell type (Gross et al., 2012), and little is known about the role of retromer in neuronal EV traffic.

Neuronal retromer localizes to cell bodies, dendrites, and axons, and is required for proper synaptic morphology, synaptic transmission, synaptic vesicle cycling, and neurotransmitter receptor and transporter traffic (Brodin and Shupliakov, 2018). In cellular and animal models of AD, loss of retromer causes mislocalization of APP and its amyloidogenic protease BACE1, leads to increased A $\beta$ , and exacerbates synaptic and cognitive defects (Brodin and Shupliakov, 2018). Retromer levels are reduced in the AD patient entorhinal cortex, and it has therefore been proposed as a therapeutic target (Berman et al., 2015). However, despite the importance of retromer in AD and endosome biology, and of endosome-derived EVs in neurological function and disease, it is unknown if or how neuronal retromer influences the traffic of APP and other cargoes into EVs. This

Department of Biology, Brandeis University, Waltham, MA.

Correspondence to Avital A. Rodal: [arodal@brandeis.edu](mailto:arodal@brandeis.edu).

© 2021 Walsh et al. This article is distributed under the terms of an Attribution–Noncommercial–Share Alike–No Mirror Sites license for the first six months after the publication date (see <http://www.rupress.org/terms/>). After six months it is available under a Creative Commons License (Attribution–Noncommercial–Share Alike 4.0 International license, as described at <https://creativecommons.org/licenses/by-nc-sa/4.0/>).



will be particularly important for retromer-directed therapies, which should target specific pathological functions of retromer rather than all of its functions.

Here, we test the hypothesis that retromer is involved in EV cargo sorting using the *Drosophila* larval neuromuscular junction (NMJ), a powerful system for studying mechanisms of synaptic EV traffic in vivo (Koles et al., 2012).

## Results

### Neuronally expressed APP trafficks into EVs

To examine trafficking of APP at synapses, we used the GAL4/UAS system to express human APP-EGFP in *Drosophila* motor neurons (Fig. 1 A). Surprisingly, in addition to its expected presynaptic localization at the NMJ, we found neuronally expressed APP-EGFP in stationary extra-neuronal puncta (Fig. 1, B and C). Since the EGFP tag is on the intracellular C terminus of APP, these puncta do not represent the shed extracellular domain of APP, but instead are likely EVs encapsulated by neuronally derived membrane. Indeed, postsynaptic APP-EGFP puncta colocalized with  $\alpha$ -HRP (which recognizes neuronal membrane glycoproteins; Snow et al., 1987), and with the neuronal EV markers Tsp42Ej (the *Drosophila* homologue of tetraspanin CD63) and Evi/Wntless (Korkut et al., 2009; Fig. 1, C and D), but not with the cytosolic presynaptic protein Complexin (Cpx; Fig. 1 B). APP-EGFP puncta were also labeled with  $\alpha$ -A $\beta$  antibodies, indicating that they contain membrane-spanning APP sequences (Fig. 1 D). Finally, we confirmed that postsynaptic puncta of neuronally driven APP-EGFP did not come from its leaky expression in muscles, since APP-EGFP expressed in muscle localized diffusely in the subsynaptic reticulum (SSR; Fig. S1 A).

We next tested if APP could sort to bona fide EVs in other cell types. We generated a stable *Drosophila* S2 cell line expressing APP-EGFP, fractionated cell culture supernatants, and immunoblotted the EV fraction for APP-EGFP. EVs pellet from cell culture supernatant at  $100,000 \times g$ , fractionate on gradients at 1.1–1.2 mg/ml sucrose, and exhibit a cup-shaped morphology by negative-stain EM (Théry et al., 2018). We found the APP-EGFP-containing EV fraction from S2 cell supernatants met these criteria (Fig. 1, E and F). Notably, a C-terminal fragment (CTF) of APP-EGFP was enriched in this EV fraction relative to full-length APP-EGFP, while EGFP alone did not fractionate with EVs. Indeed, S2 cells express proteases capable of processing APP family members (Luo et al., 1990), and similar CTFs of endogenous APP are enriched in EVs from cortical neurons (Laulagnier et al., 2018). Since CTFs are generated by endosomally localized proteases (Tan and Gleeson, 2019), this suggests that APP EVs are endosomally derived exosomes.

Finally, we asked if synaptic EV localization is conserved for the *Drosophila* APP homologue Appl, which acts as a signaling factor in neuronal development and maintenance (Cassar and Kretschmar, 2016). At wild-type and Appl-overexpressing (but not *appl*<sup>d</sup> null) NMJs, Appl  $\alpha$ -C-terminal antibodies labeled  $\alpha$ -HRP-positive extraneuronal puncta (Fig. S1, A–C). Further, cleavage-resistant Appl (Appl<sup>SD</sup>) localized to  $\alpha$ -HRP-positive extraneuronal puncta, while Appl<sup>SD</sup> lacking the C-terminal

intracellular epitope did not (Fig. S1 D), indicating that these puncta do not represent shed extracellular domain. These results suggest that EVs are a normal trajectory for synaptic APP and Appl in vivo.

### Neuronal retromer restricts accumulation of EV cargoes

At the *Drosophila* NMJ, retromer regulates synaptic vesicle size and recycling, as well as synaptic growth (Inoshita et al., 2017; Korolchuk et al., 2007; Ye et al., 2020). Retromer could also be involved in EV-mediated release of APP from neurons, as had been suggested previously in HEK293T cells (Sullivan et al., 2011), but this hypothesis has not yet been tested at synapses in vivo. To address this question, we measured APP-EGFP intensity in control and *Vps35* mutants, in the presynaptic neuron, and in EVs in the surrounding postsynaptic region. The mean intensity of APP-EGFP was strongly increased at *Vps35* mutant NMJs, in presynaptic puncta, in the overall presynaptic region, and in EVs (Fig. 2, A–C), as well as in cell bodies and axons (Fig. 2, D and E). Since synapses are a site of EV release in these neurons (Korkut et al., 2009; Korkut et al., 2013), we focused our subsequent studies on the mechanisms by which *Vps35* mutants lead to cargo accumulation and release from this site.

Using structured illumination microscopy (SIM), we found that increased presynaptic APP-EGFP levels manifested in larger and more intense puncta, rather than greater density of puncta (Fig. S2 A). Importantly, the overall increase in APP levels was insufficient to explain higher postsynaptic APP EV abundance: At both control and *Vps35* mutant NMJs, the fraction of postsynaptic APP did not correlate strongly with total (i.e., presynaptic plus postsynaptic) APP levels (Fig. S2 B). Further, the ratio of postsynaptic to total APP was significantly increased in *Vps35* mutants (Fig. S2 C). This suggests that the EV phenotype of *Vps35* mutants is mediated by a specific EV-regulatory pathway rather than simply by increased APP levels.

Retromer is ubiquitously expressed, and both neuronal and muscle retromer contribute to *Drosophila* synaptic morphology and transmission (Inoshita et al., 2017; Korolchuk et al., 2007). Indeed, endogenously tagged *Vps35*-TagRFPt (Koles et al., 2016) localizes to both neurons and muscles (Fig. 2 F). Presynaptic *Vps35*-TagRFPt was faint and difficult to resolve from postsynaptic structures, so to further explore its localization by SIM, we expressed *Drosophila* *Vps35*-HA (*Vps35*-HA) in neurons using GAL4-UAS (Fig. 2 G). *Vps35*-HA accumulated at the periphery of endosome-like structures and colocalized with a subset of APP-EGFP puncta. We then tested the cell autonomy of retromer's EV function. Neuronal restoration of *Vps35*-HA in the *Vps35* mutant background was sufficient to rescue both presynaptic and postsynaptic APP-EGFP to wild-type levels (Fig. 2, A–C). By contrast, *Vps35*-HA expression in wild-type neurons had no effect on APP levels, indicating that rescue in the mutant was not confounded by *Vps35* overexpression (Fig. S2 D). Therefore, presynaptic *Vps35* is sufficient to restrict cargo trafficking into EVs and to prevent EV cargo accumulation.

To determine the cargo specificity of retromer-dependent EV accumulation, we compared the effect of retromer loss on synaptotagmin-4 (Syt4, an established EV cargo; Korkut et al., 2013), Neuroglian (Nrg, which we confirmed is an EV cargo as

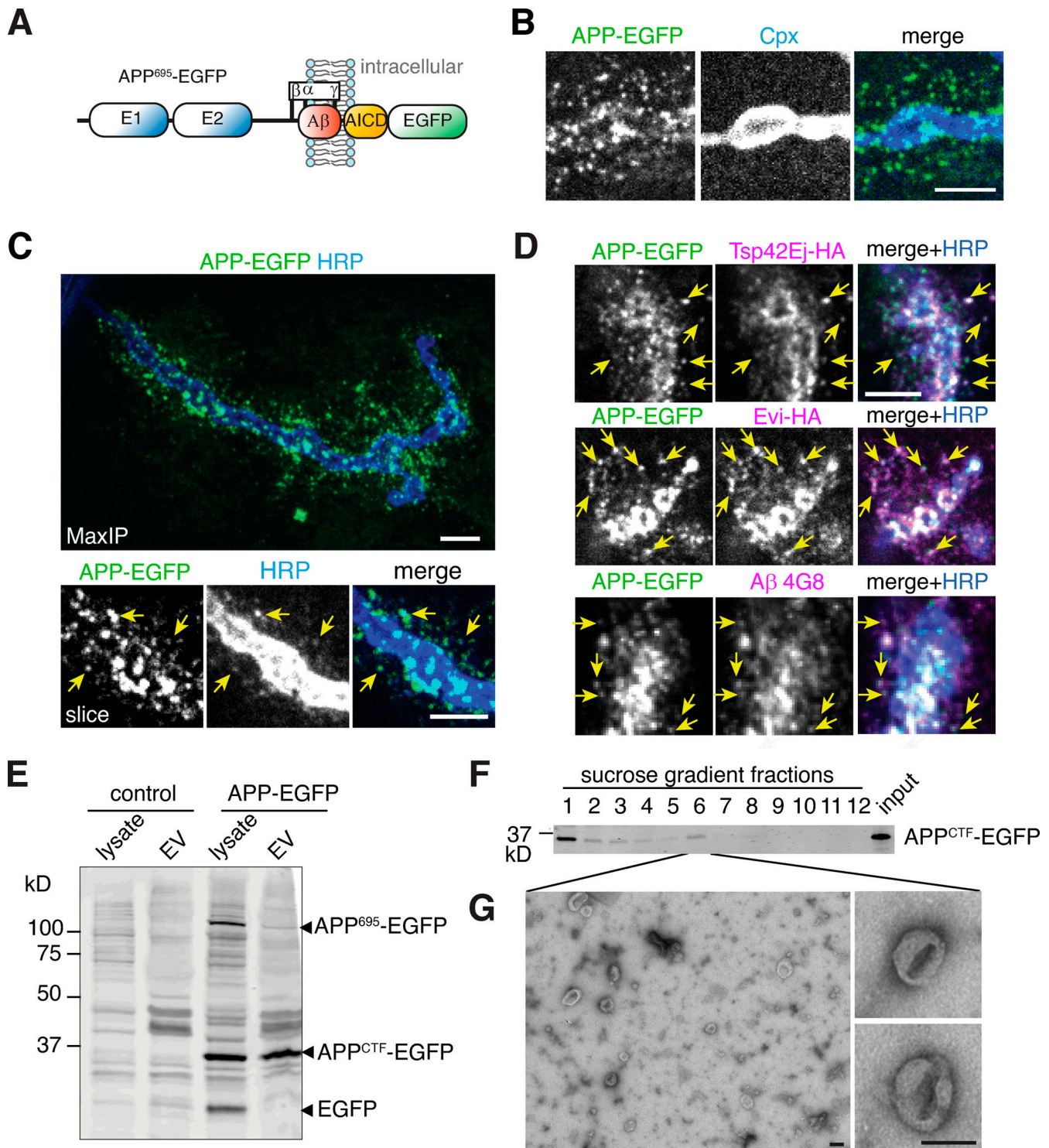
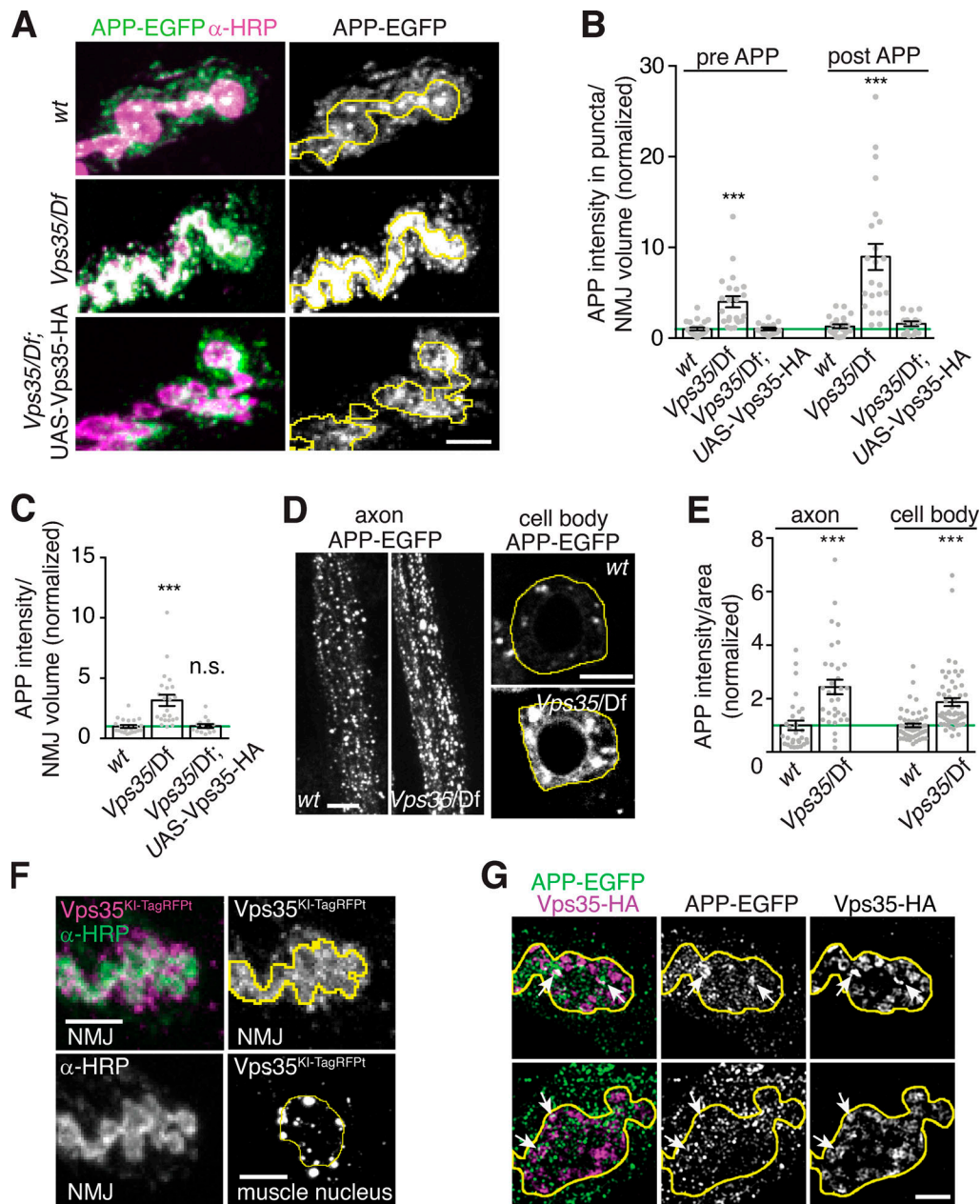


Figure 1. **APP localizes to neuronally derived EVs.** (A) Schematic of APP-EGFP construct. AICD, APP intracellular domain. (B–D) Spinning-disk confocal images from muscle 4 NMJs expressing neuronally driven UAS-APP-EGFP and labeled with the indicated antibodies. Arrows highlight examples of colocalization. (B) (MaxIP.) Motor neuron–derived APP-EGFP localizes presynaptically (marked by the cytoplasmic neuronal protein Cpx), as well as to extraneuronal puncta. (C) (MaxIP.) Motor neuron–derived APP-EGFP colocalizes pre- and postsynaptically with the neuronal membrane marker  $\alpha$ -HRP. (D) (Single confocal slices.) Motor neuron–derived APP-EGFP colocalization with neuronally expressed EV cargoes Tsp42Ej and Evi, and a transmembrane epitope in APP (4G8). Arrows highlight examples of colocalization. (E and F)  $\alpha$ -GFP immunoblots of sucrose gradient fractions from S2 cell lysates. (G) Negative-stain EM of an APP CTF-containing 1.14 mg/ml fraction. Scale bars are 5  $\mu$ m (B–D) or 100 nm (G).



**Figure 2. Neuronal retromer restricts accumulation of APP presynaptically and in EVs.** (A) MaxIPs of NMJs expressing neuronally driven UAS-APP-EGFP in the indicated genotypes. Yellow line indicates presynaptic region; scale bar is 5  $\mu$ m. (B) Quantification of presynaptic and postsynaptic (within 3  $\mu$ m of presynaptic membrane) APP-EGFP in thresholded puncta. (C) Quantification of overall (unthresholded) APP-EGFP in the presynaptic volume. (D) Single confocal slices of APP-EGFP in cell bodies in the ventral ganglion (right, outlined in yellow) and axons (left). Scale bars are 20  $\mu$ m. (E) Quantification of D. (F) Endogenously tagged Vps35-TagRFPT shows both pre- and postsynaptic localization at the NMJ (MaxIP, presynaptic terminal marked with yellow line) as well as in perinuclear puncta in the muscle (MaxIP, nucleus marked with yellow line). Scale bar is 5  $\mu$ m for NMJ and 10  $\mu$ m for muscle. (G) Partial colocalization (arrows) of APP-EGFP and Vps35-HA in MaxIPs of SIM images; presynaptic terminal marked with yellow line; scale bar is 2  $\mu$ m. Bar graphs show mean  $\pm$  SEM; n represents NMJs. See Table S3 for genotypes and statistical tests. \*\*\*,  $P < 0.001$ .

previously observed; Enneking et al., 2013; Fig. S3, A–D), and the bone morphogenetic protein receptor Thickveins (Tkv, which localizes to the presynaptic plasma membrane and endosomes and is not normally found in EVs; Deshpande et al., 2016). Endogenously tagged Syt4-EGFP exhibited increased pre- and postsynaptic accumulation in *Vps35* mutants, as well as in mutants of *Vps26*, another retromer component (Fig. 3 A). Endogenous Nrg levels were similarly increased in *Vps26* mutants,

indicating that this phenotype was not a function of the GFP tag (Fig. 3 B). Surprisingly, we observed both presynaptic and postsynaptic punctate accumulation of Tkv-mCherry in *Vps35* mutants (Fig. 3 C). Thus, retromer loss leads to the general accumulation of multiple EV and endosomal cargoes and aberrant inclusion of non-EV cargoes into EVs. By contrast, another neuronal transmembrane cargo, Synaptotagmin-1 (Syt1, which does not undergo extensive endosomal trafficking), did not

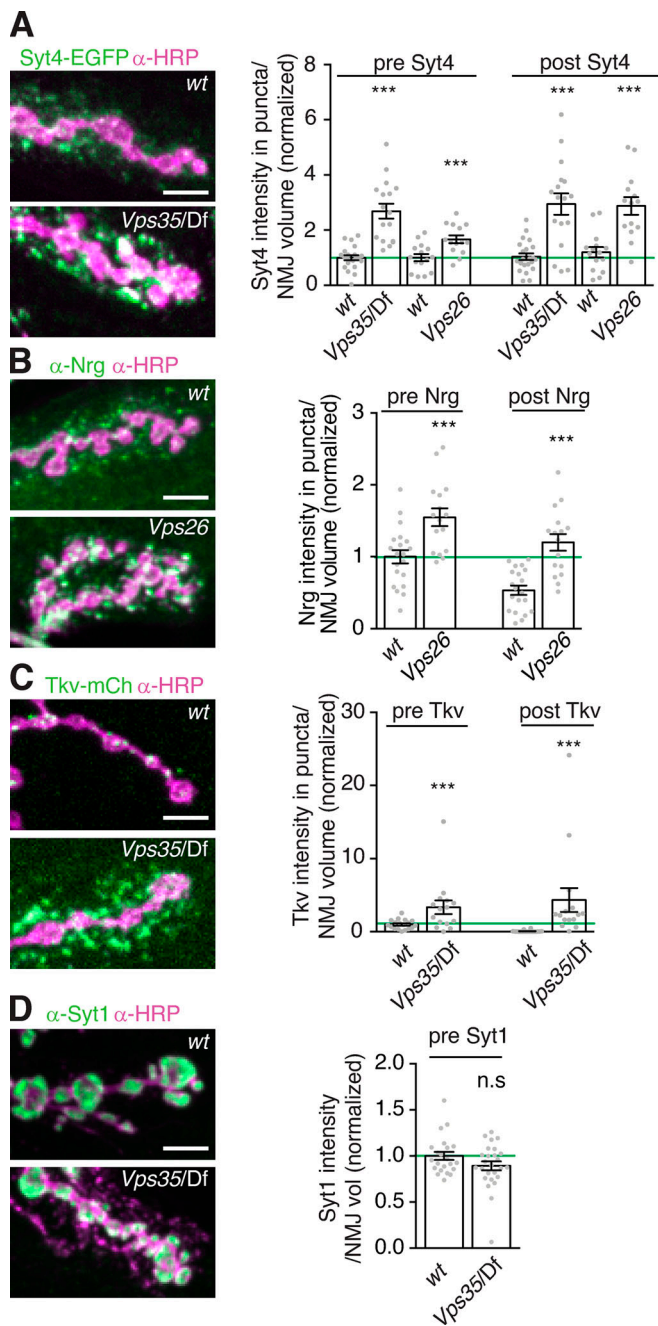


Figure 3. **Retromer mutants exhibit synaptic accumulation of multiple EV and endosomally sorted cargoes.** (A–D) Representative MaxIPs and quantification of EV cargoes Syt4-EGFP and Nrg (A and B) and non-EV cargoes Tkv-mCherry and Syt1 (C and D) in control and *Vps35* mutants. Bar graphs show mean  $\pm$  SEM; *n* represents NMJs. Scale bars are 5  $\mu$ m. All measurements were normalized to presynaptic mean of their respective control (green line). See Table S3 for genotypes and statistical tests. \*\*\*,  $P < 0.001$ .

accumulate presynaptically and was not detected in EVs in *Vps35* mutants (Fig. 3 D), indicating that retromer may specifically sequester endosomally enriched transmembrane cargoes from the EV pathway.

*Vps35* mutants may either have more EVs or else may package more cargo into the same number of EVs. To distinguish

between these possibilities, we performed EM on control and *Vps35* mutant NMJs. We noted a significant increase in post-synaptic 50–100 nm vesicles (consistent with the expected size for endosomally derived exosomes) in the muscle SSR immediately surrounding the neuron (Fig. 4, A and B), suggesting that retromer mutant NMJs release more EVs. However, we did not observe a significant increase in presynaptic MVBs (defined as structures with ILVs) or in the number or size of endosomes (defined as structures >100 nm in diameter, to distinguish them from the enlarged ~70 nm synaptic vesicles in *Vps35* mutants; Inoshita et al., 2017; Fig. 4, C–E). This result suggests that altered kinetics of MVB maturation or fusion with the plasma membrane (which would lead to MVB accumulation) is not a primary phenotype in *Vps35* mutants, or that this step may not be rate limiting for synaptic cargo and EV accumulation.

### Retromer has separable functions in synaptic growth and EV traffic

One shared function of Appl and *Vps35* is to regulate the growth of synaptic arbors during larval development (Cassar and Kretschmar, 2016; Korolchuk et al., 2007; Torroja et al., 1999; Fig. 5, A and B). We considered the possibility that synaptic overgrowth in *Vps35* mutants is caused by accumulation of synaptic growth-promoting EV cargoes. To challenge this hypothesis, we asked if we could separate the functions of retromer in EV cargo traffic and synaptic growth by genetically manipulating retromer accessory factors. Retromer acts directly or indirectly with distinct combinations of sorting nexins (SNXs) to direct specific trafficking events (Seaman, 2021). We measured synaptic growth in null mutants of *Snx27*, *Snx3*, and double mutants lacking endosomal SNX-BAR sorting complex for promoting exit 1 (ESCPE-1) complex components *Snx1* and *Snx6* (Strutt et al., 2019; Zhang et al., 2011). We found that *Snx3* mutants showed significant synaptic overgrowth, while *Snx27* single and *Snx1*, *Snx6* double mutants did not (Fig. 5, B and C). Retromer also interacts with the actin-regulating Wiskott-Aldrich Syndrome Protein and SCAR Homolog complex (Follett et al., 2014; McGough et al., 2014; Zavodszky et al., 2014), and a Parkinson’s disease-associated mutant of human *Vps35* (*Vps35*<sup>D620N</sup>) disrupts this association (Harbour et al., 2010; Jia et al., 2012; Seaman et al., 2013). Similar to previous findings (Inoshita et al., 2017; Malik et al., 2015), we found that knock-in of the analogous mutation (D628N) at the *Drosophila Vps35* locus (Koles et al., 2016) phenocopied the null mutant synaptic overgrowth (Fig. 5, A and B). Thus, SNX3 and Wiskott-Aldrich Syndrome Protein and SCAR Homolog-associated functions of retromer are required to constrain synaptic growth, while SNX27 and SNX1/6-associated functions are not.

We asked if these separable functions of *Vps35* in synaptic growth correlated with its EV cargo phenotypes. Remarkably, *Snx27* and *Vps35*<sup>D628N</sup> mutants did not phenocopy the increased EV cargo levels of *Vps35* null mutants, while *Snx1/6* double mutants recapitulated the accumulation of presynaptic and post-synaptic APP-EGFP, though to a lesser extent than *Vps35* (Fig. 6, A–C). These results demonstrate that synaptic growth and EV trafficking are distinct, uncorrelated functions of retromer that

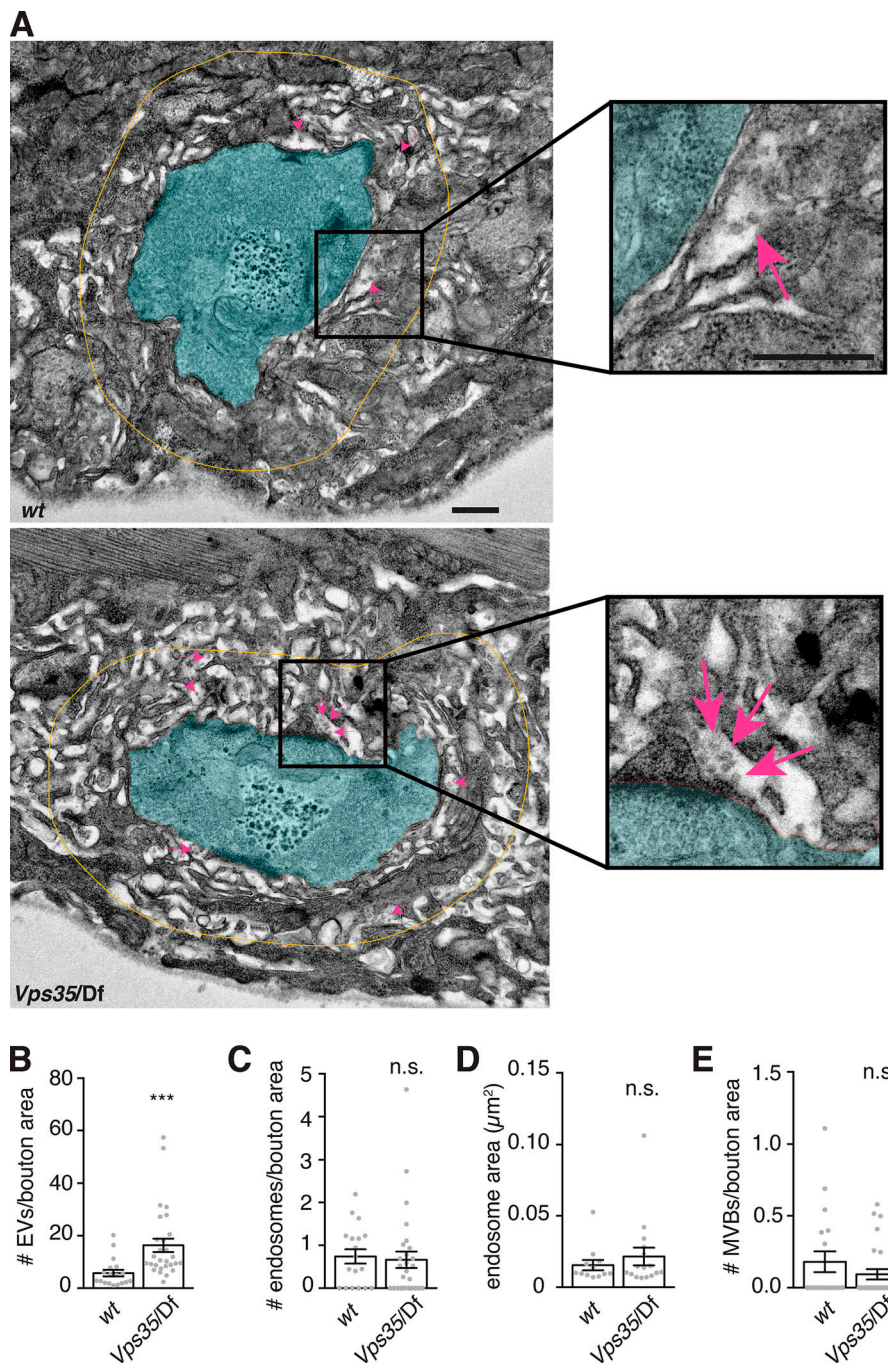


Figure 4. **Retromer mutants exhibit more EV-sized vesicles in the postsynaptic cleft, but do not exhibit changes in neuronal endosome profiles.** (A) Transmission EM of thin sections showing muscle 6/7. Boutons are pseudocolored in cyan; yellow line indicates the perimeter of the region <1  $\mu\text{m}$  from bouton plasma membrane, in which 40–100-nm vesicular structures were counted in the extracellular space. Magenta arrows indicate several examples of such EV-sized structures. Scale bar is 500 nm. (B) *Vps35* mutants exhibit a greater number of 50–100-nm EV-sized vesicles in the postsynaptic cleft. (C and D) However, neither the number (C) nor size (D) of presynaptic endosomes (>100-nm vesicles) increases in a *Vps35* mutant. (E) Presynaptic MVBs are rare at both control and *Vps35* mutant synapses. Bar graphs show mean  $\pm$  SEM; each data point represents measurements derived from a single bouton. See Table S3 for genotypes and statistical tests. \*\*\*,  $P < 0.001$ .

can be genetically uncoupled, and that rely on separate components of the *Vps35*-associated machinery.

### Lysosome dysfunction does not recapitulate *Vps35* EV phenotypes

We next investigated the mechanisms by which loss of retromer results in increased levels of EV cargo. Since retromer is required to maintain lysosomal hydrolase activity (Arighi et al., 2004; Cui et al., 2019; Seaman et al., 1998), general lysosomal dysfunction in retromer mutants might lead to the accumulation and release of material that would otherwise be targeted for degradation (Bécot et al., 2020). We tested this by examining the lysosomal marker Spinster (Spin; Dermaut et al., 2005; Sweeney

and Davis, 2002). Spin-GFP intensity was significantly reduced at *Vps35* mutant NMJs (Fig. S4, A and B), arguing against lysosomal expansion, and consistent with the absence of enlarged lysosomal profiles in our EM data. We next asked if lysosomes were functionally impaired in *Vps35* mutants by measuring the levels of Atg8-GFP, a marker of autophagosomes, which accumulate during lysosomal dysfunction. Instead, we observed a significant decrease in Atg8-GFP intensity in *Vps35* NMJs (Fig. S4, A and B). Finally, staining with LysoTracker Deep Red, which labels acidic compartments, was reduced in *Vps35* mutant muscle (Fig. S4 C), and undetectable in control or *Vps35* mutant presynaptic terminals, again suggesting that acidic compartments are not amplified at *Vps35* mutant NMJs. These results

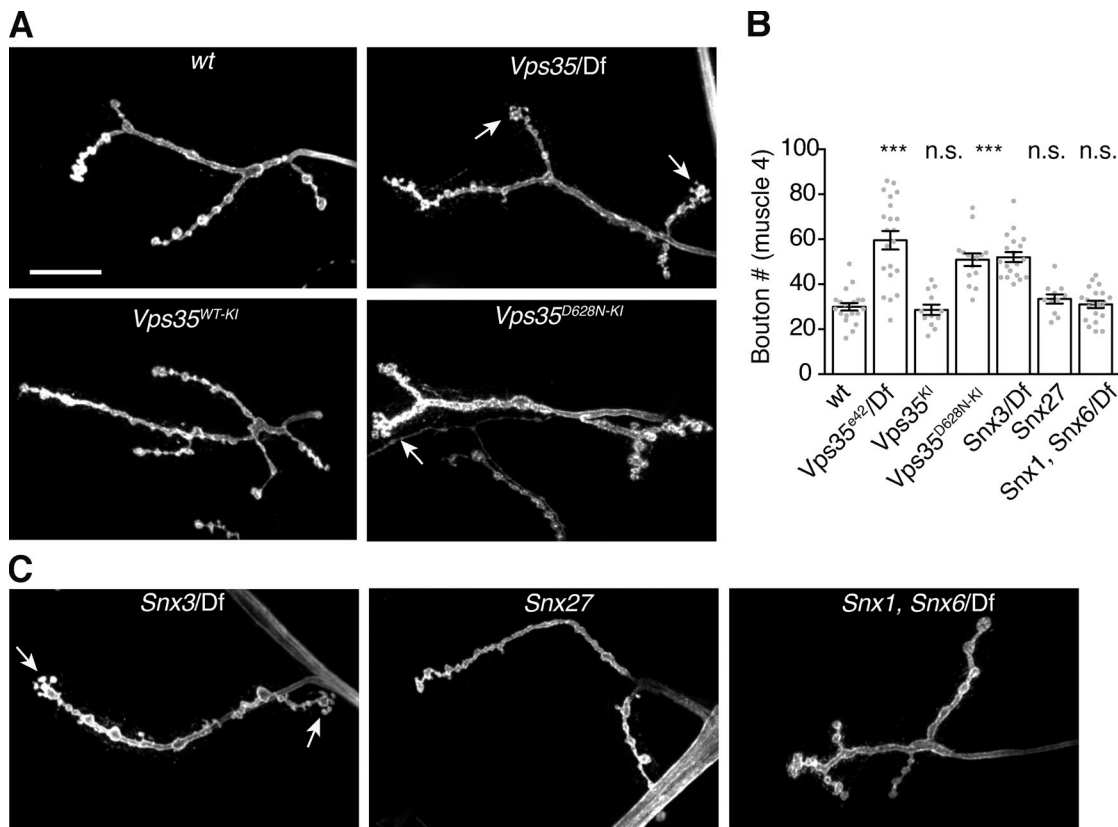


Figure 5. **Control of synaptic growth depends on specific retromer-associated pathways.** *Vps35* null, *Snx3*, and *Vps35<sup>D628N</sup>* mutations cause an increase in bouton number at the NMJ, while mutations in retromer-associated *Snx1*, *Snx6*, and *Snx27* have no effect. **(A)** MaxIPs of  $\alpha$ -HRP-labeled muscle 4 NMJs in the indicated genotypes. Scale bar is 20  $\mu$ m. **(B)** Quantification of bouton number for muscle 4, segments A2 and A3. **(C)** MaxIPs of  $\alpha$ -HRP-labeled muscle 4 NMJs in the indicated genotypes. Scale is identical to A. See Table S3 for detailed genotypes and statistical tests. \*\*\*,  $P < 0.001$ .

contrast with previous findings of increased LysoTracker and Atg8 fluorescence in *Drosophila Vps35* mutant fat body cells (Maruzs et al., 2015), and suggest that unlike in other tissues, *Vps35* mutant synapses do not accumulate acidified endolysosomes.

We then asked if disruption of lysosomal function affected EV cargo traffic similarly to the *Vps35* mutant. We measured pre- and postsynaptic Syt4-EGFP levels in mutants of *spin* and *deep orange* (*dor/Vps18*), which are both required for lysosome function at the NMJ (Dermaut et al., 2005; Fernandes et al., 2014; Narayanan et al., 2000; Sweeney and Davis, 2002). In contrast to elevated Syt4-EGFP levels in *Vps35* mutant NMJs, pre- and postsynaptic Syt4-EGFP were significantly reduced in *spin* and *dor* mutant NMJs compared with controls (Fig. S4, D and E). Finally, we pharmacologically disrupted lysosome function with chloroquine, which blocks lysosome acidification (Gonzalez-Noriega et al., 1980). Chloroquine treatment caused a decrease in larval viability as well as enlarged presynaptic Syt4-EGFP puncta, indicating lysosome dysfunction. However, Syt4-EGFP levels did not change either pre- or postsynaptically (Fig. S4, F and G). Taken together, these results suggest that defects in the lysosomal pathway do not promote EV cargo accumulation in *Vps35* mutants.

#### A Rab11-dependent recycling pathway maintains EV cargo levels

Since generalized endolysosomal dysfunction is unlikely to account for *Vps35* EV phenotypes, we next asked whether and how specific subtypes of endosomes were altered in *Vps35* synapses. We examined the localization and levels of Rab GTPases implicated in retromer function, using antibodies or tags knocked in to their endogenous loci (Fig. 7 A). GFP-Rab5, which is associated with early endosomes, showed a decrease in mean puncta intensity and number (but not size) in *Vps35* mutant NMJs compared with controls (Fig. 7, B–D). By contrast, YFP-Rab7, which is associated with late endosomes, showed an increase in intensity, puncta number, and puncta size in both *Vps35* (Fig. 7, B–D) and *Vps26* (Fig. S5 A) mutants. This indicates an amplification of late endosomes, consistent with the role of retromer in attenuating Rab7 activity (Jimenez-Organ et al., 2018; Kvainickas et al., 2019; Seaman et al., 2018; Ye et al., 2020). Levels of  $\alpha$ -Rab11 immunostaining, marking the recycling endosome and post-Golgi secretory vesicles, remained unchanged, but Rab11 structures increased in size (but not number) in *Vps35* (Fig. 7, A, B, and E–G) and *Vps26* (Fig. S5 B) mutants. Thus, one or several of these endosomal changes might underlie retromer-dependent EV trafficking

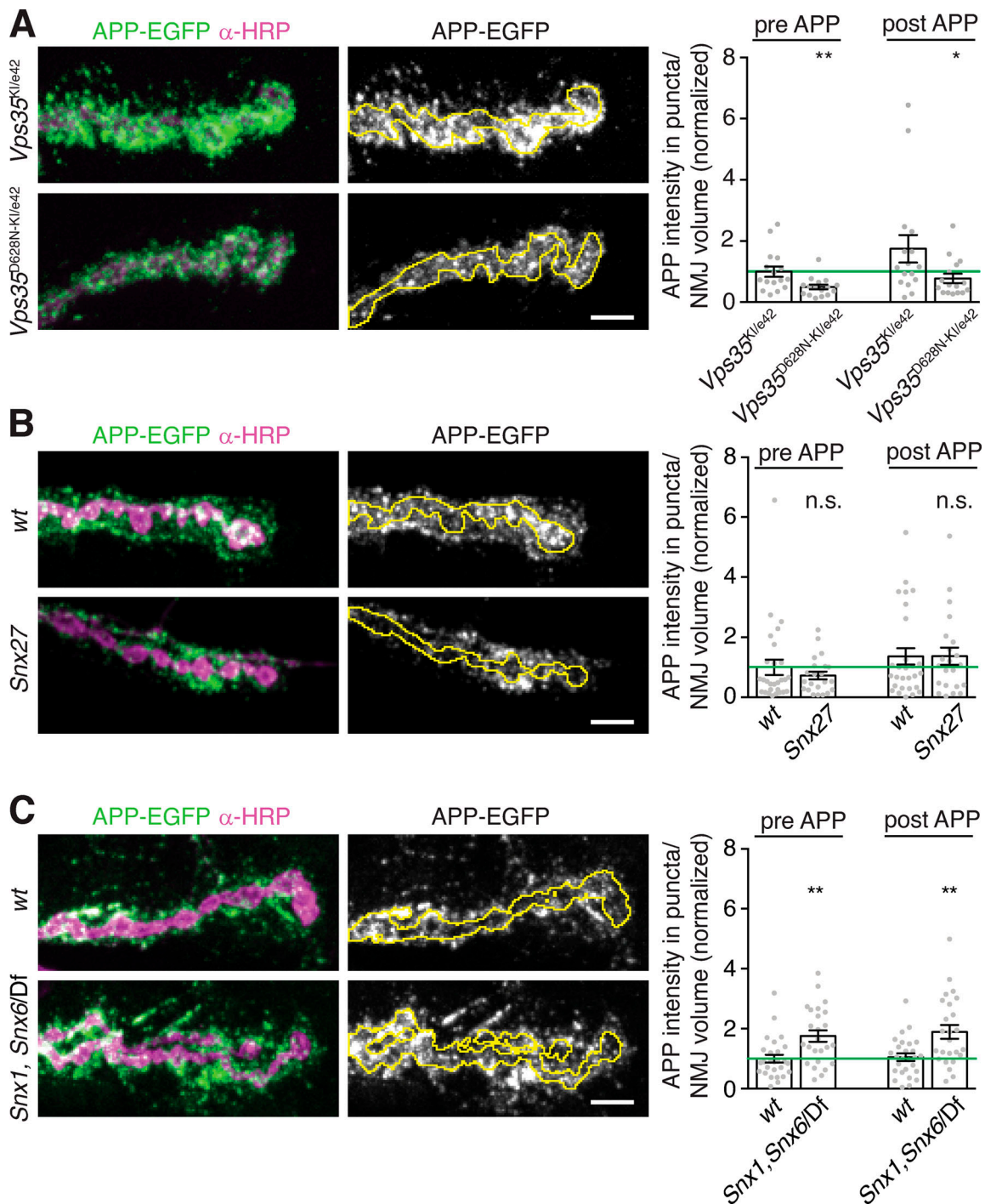


Figure 6. **Control of EV Cargo levels depends on the Snx1/Snx6 ESCPE-1 complex but not *Vps35<sup>D628N</sup>* or *Snx27*.** (A–C) Representative MaxIPs and quantification of APP-EGFP levels at muscle 6/7 NMJs in the indicated genotypes. Each condition is normalized to the mean intensity of wild-type control (green line). Bar graphs show mean  $\pm$  SEM; dots show all data points representing individual NMJs. Yellow line indicates presynaptic region; scale bars are 5  $\mu$ m. See Table S3 for detailed genotypes and statistical tests. \*,  $P < 0.05$ ; \*\*,  $P < 0.01$ .

phenotypes and define the site at which EV cargo fate is determined.

We then separately perturbed the function of each type of endosome using neuron-specific expression of constitutively active (CA) or dominant negative (DN) forms of their resident Rab GTPases and measured pre- and postsynaptic levels of Syt4-EGFP (Fig. 8, A–D). Overexpression of Rab5<sup>CA</sup>, which promotes

homotypic fusion but blocks conversion to the Rab7-positive state (Rink et al., 2005; Stenmark et al., 1994), did not change presynaptic Syt4 levels, although Syt4 was redistributed into aberrant bright puncta. Notably, we observed decreased EVs in this condition. This suggests that trapping cargo in early endosomes inhibits EV release, and that retromer sorts cargo away from the EV pathway downstream of Rab5. Overexpression of

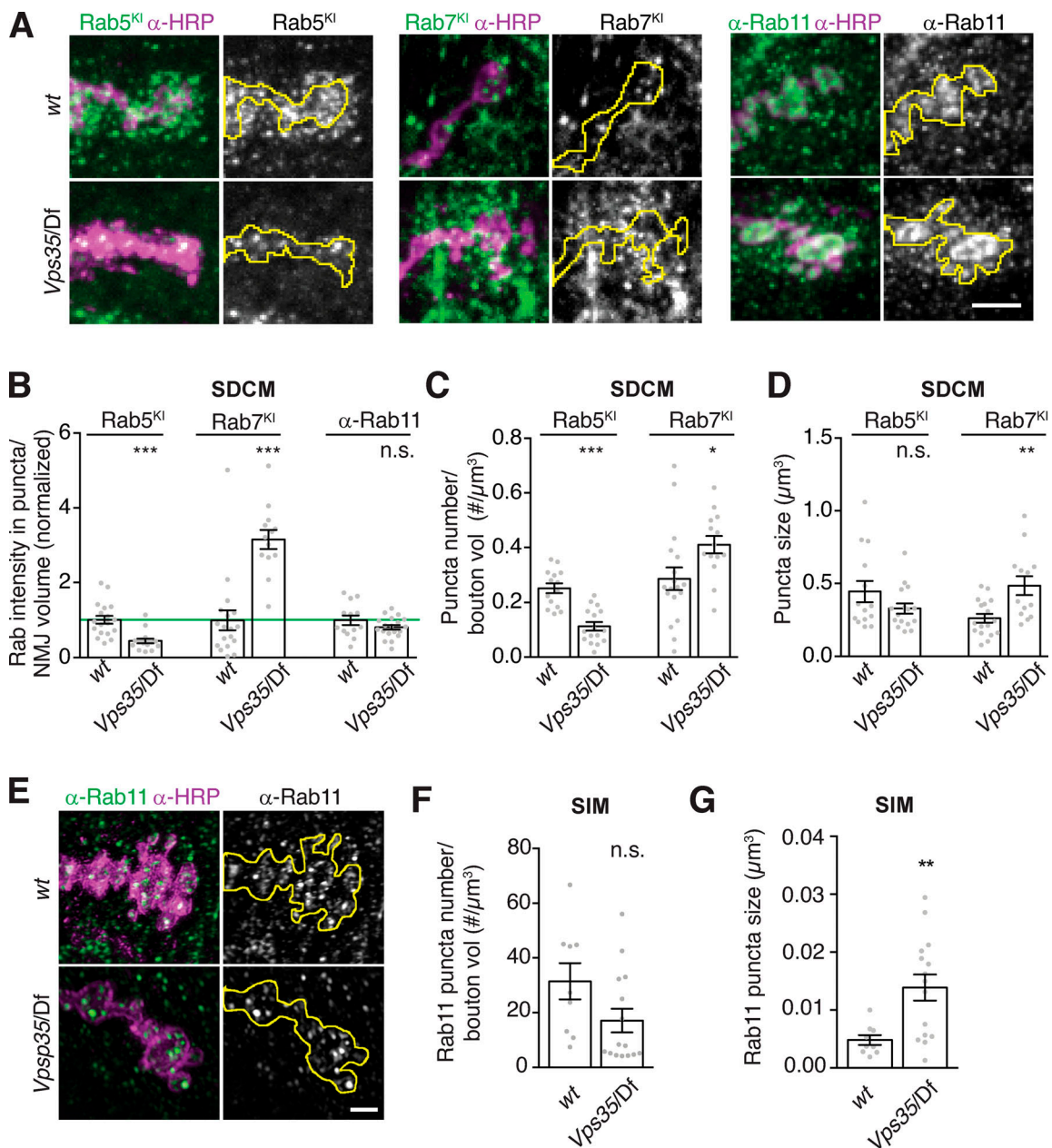


Figure 7. **Endosome distribution in *Vps35* mutants.** (A) MaxIPs of confocal images of NMJs from larvae expressing endogenously tagged YFP-Rab7 or GFP-Rab5, or labeled with  $\alpha$ -Rab11 antibodies, in control or *Vps35/Df* genotypes. (B) Quantification of fluorescence intensity from spinning-disk confocal microscopy (SDCM), normalized to mean intensity of wild-type control (green line). (C) Rab5 and Rab7-positive puncta density by SDCM. (D) Rab5 and Rab7-positive puncta size by SDCM. (E) SIM MaxIPs of NMJs from control or *Vps35/Df* genotypes, labeled with  $\alpha$ -Rab11 antibodies. Rab11 puncta were too dense to distinguish by SDCM, so we used SIM to analyze individual endosomes. (F and G) Quantification of puncta density and size from E. Scale bars are 5  $\mu$ m for SDCM, 2  $\mu$ m for SIM. Presynaptic terminal marked with yellow line; bar graphs show mean  $\pm$  SEM; dots show all data points representing individual NMJs. See Table S3 for genotypes and statistical tests. \*,  $P < 0.05$ ; \*\*,  $P < 0.01$ ; \*\*\*,  $P < 0.001$ .

Rab5<sup>DN</sup> blocks homotypic endosome fusion and impairs early endosome maturation (Stenmark et al., 1994), so we used this manipulation to test if the decreased Rab5 levels that we observed in *Vps35* mutants could account for increased EV cargo levels. Indeed, we saw a twofold increase in presynaptic Syt4 levels, similar to *Vps35* mutants. However, unlike *Vps35* mutants, postsynaptic Syt4 was unaffected (Fig. 8, A and C). Thus, though inhibiting Rab5 function causes accumulation of EV cargoes in the presynaptic neuron, it does not affect release of these

cargoes in EVs. This supports our previous conclusion that accumulation of cargo alone is not sufficient to drive EV sorting (Fig. S2 B), and further suggests that reduction in Rab5 levels in *Vps35* mutants is unlikely to account for EV cargo sorting phenotypes.

Manipulations of Rab7 had a milder influence on Syt4 trafficking compared with Rab5. Overexpression of Rab7<sup>CA</sup> caused a modest decrease in EV Syt4 (Fig. 8, A and C). Rab7<sup>CA</sup> increases the rate by which the late endosome merges with the lysosome

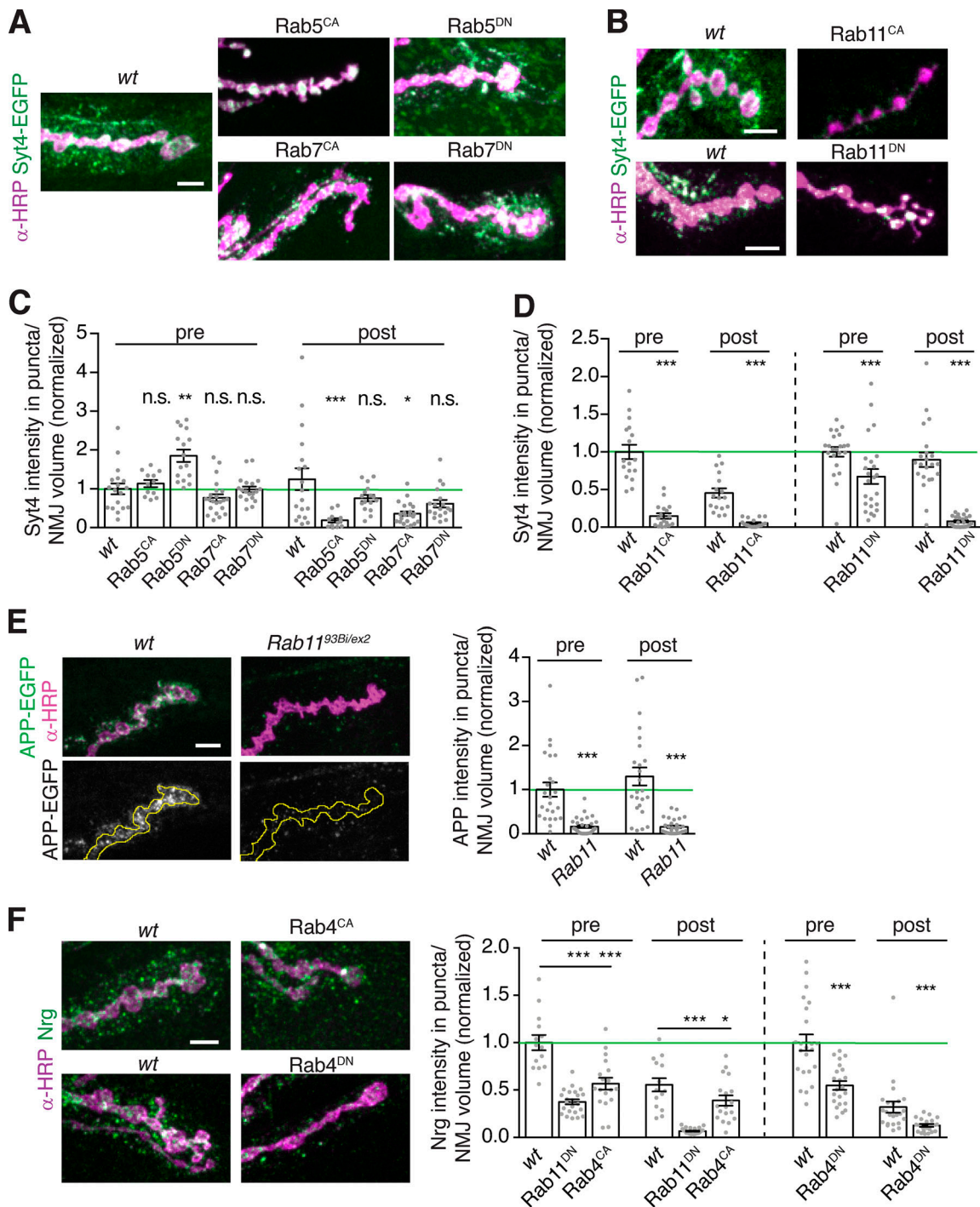


Figure 8. **EV cargo accumulation depends on Rab11 and Rab4 activity.** (A and B) MaxIPs and quantification of NMJs from larvae expressing endogenously tagged Syt4-EGFP with neuronally driven (GAL4<sup>C380</sup>) Rab5, Rab7, and Rab11 transgenes. (C and D) Quantification of A and B. (E) MaxIPs and quantification of NMJs expressing APP-EGFP in control or Rab11 mutant backgrounds. Control dataset is identical to that in Fig. 2 B. Yellow line indicates presynaptic region. (F) MaxIPs and quantification of NMJs from larvae with neuronal GAL4<sup>glut</sup>-driven YFP-Rab11 and YFP-Rab4 transgenes. All bar graphs show mean ± SEM; independent experiments are shown separately, each normalized to the mean presynaptic intensity of their respective wild-type controls (green line). Dots show all data points representing individual NMJs. Scale bars are 5 μm. See Table S3 for detailed genotypes and statistical tests. \*, P < 0.05; \*\*, P < 0.01; \*\*\*, P < 0.001.

(Méresse et al., 1995), so this phenotype may reflect accelerated degradation of EV cargoes. Rab7<sup>DN</sup> overexpression, which inhibits recruitment of Vps35 to late endosomes (Rojas et al., 2008; Seaman et al., 2009) and prevents the Rab5-to-Rab7 switch that

is a hallmark of endosome maturation (Rink et al., 2005), had no effect on pre- or postsynaptic Syt4 levels (Fig. 8, A and C). Finally, we examined the Rab7 compartment in *Snx1*, *Snx6* ESCPE-1 double mutants, which exhibit increased EV cargo levels.

Rab7-positive endosome intensity, size, and number were not significantly different from wild-type in ESCPE-1 mutants (Fig. S5 C). Together, these data argue that the accumulation of Rab7 and Rab7-associated compartments in *Vps35* mutant is unlikely to be necessary for the EV cargo trafficking defect, and that synaptic EV cargo sorting does not depend on recruitment of *Vps35* to late endosomes by Rab7.

Next, we examined the effects of manipulating Rab11. DN and loss-of-function alleles of Rab11 block recycling of endosome- and Golgi-derived carriers to the plasma membrane (Ullrich et al., 1996) and reduce EV levels of the transferrin receptor (TfR), Evi, Syt4, and Arc (Ashley et al., 2018; Beckett et al., 2013; Koles et al., 2012; Korkut et al., 2013; Savina et al., 2002). This led to the hypothesis that Rab11 is involved in MVB fusion with the plasma membrane, and the prediction that EV cargoes should accumulate presynaptically in Rab11 mutants, though this has not yet been directly tested. Surprisingly, opposite to this prediction, we found decreased pre- and postsynaptic Syt4-EGFP upon Rab11<sup>DN</sup> expression (Fig. 8, B and D), as well as APP-EGFP in a hypomorphic *rab11* loss-of-function allelic combination (Fig. 8 E). By contrast, we previously found that Rab11<sup>DN</sup> has no effect on presynaptic levels of the non-EV cargo Tkv, indicating that this depletion is specific to EV cargo (Deshpande et al., 2016). Constitutively active Rab11 (Rab11<sup>CA</sup>) is predicted to enlarge the recycling endosome and also disrupts recycling activity (Ullrich et al., 1996; Wilcke et al., 2000). We found that neuronal expression of Rab11<sup>CA</sup> dramatically altered neuronal morphology including reduced  $\alpha$ -HRP staining, synaptic bouton size, and overall arbor size (as previously described; Akbergenova and Littleton, 2017). With the caveat that this extreme phenotype likely causes pleiotropic defects in membrane traffic, Syt4-EGFP levels were also reduced both presynaptically and postsynaptically in Rab11<sup>CA</sup>-expressing animals. Finally, we examined the “fast recycling” pathway mediated by Rab4 (D’Souza et al., 2014). Rab4<sup>CA</sup> and Rab4<sup>DN</sup> both caused significant reductions in Nrg levels both pre- and postsynaptically, similar to Rab11 (Fig. 8 F), indicating that Rab4 and Rab11 pathways may act together or in parallel. Since multiple recycling pathway manipulations caused EV phenotypes opposite from *Vps35* mutants, we hypothesized that recycling may regulate EV cargo levels by counteracting the *Vps35* pathway, and further investigated the role of Rab11 compartments in the *Vps35* mutant phenotype.

#### APP accumulates in a Rab11-dependent compartment in *Vps35* mutants

Depending on the specific cell type and cargo, loss of retromer can result in altered cargo levels in early endosomes, in late endosomes, or on the plasma membrane (Seaman, 2021). The specific site of cargo accumulation at *Vps35* mutant synapses may thus reveal which compartments are EV permissive in neurons. Our genetic data indicated that this may be the Rab11 compartment, so we asked if retromer regulates APP traffic through presynaptic Rab11-positive structures. In control animals, APP-EGFP and Rab11 partially colocalized by SIM (Fig. 9 A), and in *Vps35* mutants, we found an increased fraction of Rab11 signal in APP-positive compartments (Fig. 9, A–C). These data suggest

that when EV cargo is retained in a recycling regimen, it is more likely to be incorporated into EVs.

We then asked whether aberrant sorting of EV cargo through this Rab11-positive compartment in *Vps35* mutants caused this accumulation, by testing if levels could be restored by rebalancing the opposing activities of Rab11 and *Vps35* in *Vps35*; *rab11* double mutants. *rab11* null mutants are embryonic lethal (Dollar et al., 2002), precluding clean epistasis experiments, so we tested how these mechanisms interact using hypomorphic mutants. Strikingly, reduction of *rab11* function in the *Vps35* mutant significantly rescued both pre- and postsynaptic Syt4 and Nrg levels (Fig. 9, D and E). These results suggest that accumulation of Syt4 in a Rab11-dependent compartment (possibly in the Rab11-positive compartment itself) in *Vps35* mutants is causative of EV cargo accumulation and release. Finally, to ask whether Rab11 and *Vps35* might be acting on the same compartment, we performed SIM and found Rab11-*Vps35*-positive puncta in all NMJs we examined ( $n = 8$ ; Fig. 10 A).

## Discussion

Here we find that trafficking of multiple synaptic EV cargoes is restricted by the neuron-autonomous activity of retromer. Rather than playing a general role in maintaining overall endolysosomal homeostasis, we find that retromer has separable roles in neurons and specifically restricts traffic within the EV pathway by regulating accumulation of cargoes in Rab4/Rab11-dependent endosomes. Our results indicate that retromer and Rab4/Rab11 recycling balance traffic of AD-relevant cargoes such as APP into the EV pathway, and may therefore be critical for disease propagation in the brain.

#### Neuronal retromer has multiple, separable functions

Our EV trafficking findings add to the retromer’s previously described roles in synaptic morphogenesis and transmission, synaptic vesicle loading and recycling, and neurotransmitter receptor and transporter traffic (Brodin and Shupliakov, 2018). Interestingly, photoreceptor degeneration and synaptic transmission defects in retromer mutants are opposed by Rab11, similar to our findings for EV phenotypes, suggesting that balance between these pathways is of general importance in neurons (Inoshita et al., 2017; Satoh et al., 2005; Wang et al., 2014). However, our data also show that the role of retromer in EV traffic is separable from its other functions. Compared with synaptic transmission and synaptic growth defects, which require both neuronal and muscle retromer (Inoshita et al., 2017; Korolchuk et al., 2007), presynaptic retromer is sufficient for EV cargo regulation. Further, synaptic growth, Rab7 endosome maturation, and EV defects are genetically separable: *Snx3* and *Vps35*<sup>D628N</sup> mutants phenocopy *Vps35* null mutants for synaptic growth (likely via excess bone morphogenetic protein signaling; Korolchuk et al., 2007) but not for EV traffic, while ESCPE-1 mutants recapitulate EV but not synaptic growth or Rab7 turnover phenotypes of *Vps35*.

Given these diverse phenotypes, it will be critical to determine which of these many cellular functions of retromer underlie neurological disease. Indeed, acute depletion of *Vps35* in



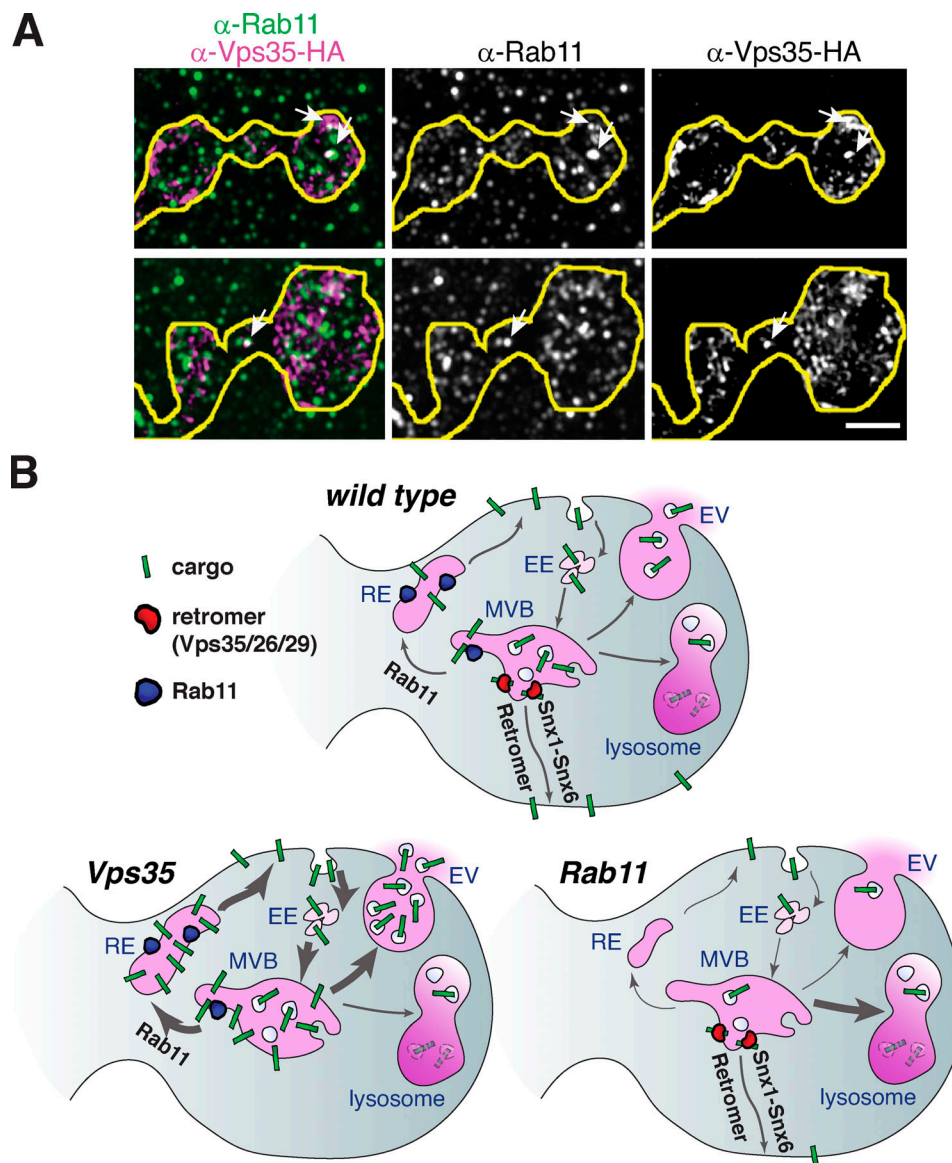


Figure 10. **Synaptic Vps35 and Rab11 compartments and model.** (A) Vps35 and Rab11 colocalize on a subset of endosomes. MaxIP SIM images from NMJs expressing neuronally driven Vps35-HA immunolabeled for  $\alpha$ -HA and  $\alpha$ -Rab11. Yellow line indicates presynaptic region; arrows indicate Vps35-HA and Rab11-positive structures. Scale bar is 2  $\mu$ m. (B) Model for the balance of retromer-mediated removal and recycling traffic in populating the EV pathway. EV cargo is maintained in a recycling pool between the early endosome (EE), the recycling endosome (RE), and the plasma membrane. MVBs populated by this pathway preferentially fuse with the plasma membrane and release their contents as EVs. In *Vps35* mutants, cargo is retained in the recycling pathway. Increased levels of cargo on the endosome membrane may drive ILV formation, resulting in EV secretion and pre- and postsynaptic cargo accumulation. In a *rab11* mutant, the recycling pool of cargo is not maintained. Cargo proceeds to the lysosome for degradation and is depleted from the synapse.

and individually manipulating these functions via distinct retromer-associated molecular pathways may improve therapeutic strategies (Berman et al., 2015).

#### Retromer and Rab4/Rab11-dependent mechanisms of EV traffic in neurons

Our data highlight the importance of studying the cell biological functions of retromer in neurons in vivo. The canonical role of retromer is to rescue endosomal cargoes from lysosomal degradation and to redirect them to the Golgi or plasma membrane; in many cell types, retromer loss causes these cargoes to be misrouted to the lysosome and degraded (Arighi et al., 2004; Cui

et al., 2019; Seaman et al., 1998; Steinberg et al., 2013; Temkin et al., 2011). By contrast, we observe accumulation of cargoes in *Vps35*-deficient *Drosophila* neurons, similar to hippocampal neurons (Bhalla et al., 2012) and secretory cells of the *Drosophila* salivary gland (Neuman et al., 2021). A prevailing hypothesis that could account for this accumulation is retromer-dependent lysosome dysfunction (Maruzs et al., 2015; Miura et al., 2014; Wang et al., 2014). Indeed, lysosomal damage increases APP-CTFs in secreted EVs from neuroblastoma cells (Miranda et al., 2018; Vingtdoux et al., 2007). However, in our in vivo system, we did not observe functional or ultrastructural indications of lysosome defects. Further, manipulating late endosome or

lysosome function did not phenocopy retromer loss, suggesting that, like salivary gland secretory cells (Neuman et al., 2021), lysosome dysfunction is not sufficient to account for the observed cargo increase at synapses (though we cannot exclude a contributing role). Finally, we found that retromer-mediated Rab7 turnover and late endosome maturation is unlikely to be involved in synaptic EV traffic, though Rab7 does contribute to EV release in other neuronal cell types (Song et al., 2016).

Our data instead suggest that in retromer mutant neurons, endosomal cargoes are diverted to the EV pathway, rather than to lysosomal degradation. This could be beneficial, since EV recipient cells (i.e., muscles and glia) may be better suited for cargo degradation than the donor neuron, which has limited lysosomal capability (Eitan et al., 2016; Ferguson, 2018; French et al., 2017; Fuentes-Medel et al., 2009). According to this model, in presynaptic nerve terminals, MVBs would preferentially fuse with the plasma membrane rather than with lysosomes. Why, then, do we not observe excess MVBs by EM in retromer mutants, and why do EV cargoes accumulate in Rab11-positive compartments?

We propose that EV traffic is not rate limited by MVB–plasma membrane fusion (Lauwers et al., 2018), but instead by loading of endosomes with EV cargo via recycling pathways (Fig. 10 B). This mechanism may be conserved, as EV-directed p75-neurotrophin receptor accumulates in Rab11-positive compartments in PC12 cells and sympathetic neurons (Escudero et al., 2014). Rab11 has previously been implicated in the MVB–plasma membrane fusion step of EV traffic (Escudero et al., 2014; Fan et al., 2020; Koles et al., 2012; Korkut et al., 2013; Savina et al., 2002). Our results instead show that the primary cause of EV trafficking defects in *rab11* mutants is cargo depletion in the donor cell (as observed for the EV cargo Arc; Ashley et al., 2018). We hypothesize that recycling maintains a pool of EV cargo that fluxes between early endosomes, recycling endosomes, and the plasma membrane; this recycling pool of cargo is protected from lysosomal degradation and is incorporated into MVBs destined to become EVs. Alternatively, recycling cargo could be released from the plasma membrane by direct budding of microvesicles. An alternative hypothesis is that the recycling pathway directly loads cargo into Rab11-positive MVBs, similar to EV-releasing *Drosophila* accessory gland secondary cells (Corrigan et al., 2014; Fan et al., 2020; Marie et al., 2020 Preprint).

Retromer may oppose EV formation in several ways: It might retrieve or protect cargo from Rab11-dependent trafficking through the recycling endosome (perhaps via direct recycling to the plasma membrane; Naslavsky and Caplan, 2018; Steinberg et al., 2013), either by interacting directly with cargo (Simonetti et al., 2017) or via carriers such as SorLA (Fjorback et al., 2012; Nielsen et al., 2007). Our finding that ESCPE-1 acts in EV traffic may enable identification of EV cargo sorting determinants, given recent insights into SNX1–SNX6–dependent sorting motifs (Simonetti et al., 2019; Yong et al., 2020). In support of direct sorting, we found that Rab11 and Vps35 partly colocalize at the synapse. It will also be interesting to further unravel the role of Rab4 in this process, and ask if it acts in parallel or together with Rab11. Alternatively, retromer may nonspecifically restrict MVB formation by creating domains protected from ESCRT-mediated

ILV formation (Derivery et al., 2012; Norris et al., 2017), or by limiting overall cargo accumulation on endosomes, thus suppressing ESCRT activity (Baietti et al., 2012). In support of this indirect role, we found an overall increase in EV-like postsynaptic structures in *Vps35* mutants, as well as aberrant trafficking of the non-EV cargo Tkv into EVs.

### Role of the retromer-Rab11 EV pathway in neuronal function and disease

Our results have implications for the role of Vps35 in human disease. We found that the Parkinson's disease *Vps35*<sup>D628N</sup> mutant does not recapitulate *Vps35* null EV trafficking defects. Instead, our results may relate more directly to AD, which is associated with reduced levels of retromer, based on genetic and pathological data from patients (Small et al., 2005; Vardarajan et al., 2012), and findings that *Vps35* mutants enhance pathology in AD animal models (Li et al., 2020; Muhammad et al., 2008; Wen et al., 2011). The specific role of retromer in APP traffic is unclear, due to differing results for trafficking itineraries and intersections of APP and its processing proteases in various cell types (Arbo et al., 2020; Tan and Gleeson, 2019). In neurons, loss of retromer increases colocalization of APP and BACE1 in early and late endosomes, resulting in higher A $\beta$  levels (Bhalla et al., 2012; Toh et al., 2017; Wang et al., 2012a; Wen et al., 2011). Our results now extend the role of neuronal retromer to the EV pathway, and show that retromer loss promotes traffic of endosomally derived APP CTFs into synaptic EVs, potentially driving intercellular propagation of A $\beta$ , and other EV cargoes such as tau (Kanmert et al., 2015).

Conversely, Rab11 is also genetically linked to AD, but exhibits the opposite behavior from *Vps35*: Rab11 loss causes decreased A $\beta$ , while Rab11 activation causes increased A $\beta$  (Li et al., 2012; Udayar et al., 2013). These effects were previously ascribed to Rab11-mediated intracellular traffic (e.g., by regulating the endocytosis of A $\beta$  and trafficking of BACE1; Buggia-Prévoit et al., 2014; Li et al., 2012; Udayar et al., 2013). Our data suggest a new interpretation of these previous disease model results; loss of Rab11 may suppress AD phenotypes by counteracting pathological EV cargo traffic and shunting synaptic APP for degradation.

What, then, is the physiological function of the retromer-dependent EV pathway? Our results suggest that an important role of EV traffic is to deliver neuronal cargo to recipient cells for disposal, as an alternative to intraneuronal lysosomal degradation. However, increasing evidence suggests that neuronal EV cargoes also play functional roles in recipient cells, driving structural and functional plasticity as well as morphogen signaling (Holm et al., 2018). In the future, it will be exciting to test whether neurons control these functional processes by directly tuning EV traffic via the endosomal machinery, lending these trafficking mechanisms interesting new roles beyond general synaptic proteostasis.

## Materials and methods

### *Drosophila* strains and methods

To create human APP-EGFP, the APP<sup>695</sup> isoform was cloned into pBI-UASc-gateway-EGFP (Wang et al., 2012b) and injected into

flies using  $\Phi$ c381 recombinase at the Attp40 locus (Ni et al., 2008). The endogenous Syt4 locus was tagged with a tissue-specific convertible TagRFPT to EGFP tag (T-STEP; Koles et al., 2016). Briefly, the following genomic sequence was used to target DNA cleavage by Cas9: 5'-TGAACGAGTAGGGGAGGGGC-3' (at location 3R:7269302-7269321), with the 5' T converted to the obligatory G, thus yielding the 20-bp sequence 5'-GGAACGAGTAGGGGAGGGGC-3'. The T-STEP cassette was flanked with 5' homology (3R: 7267814-7269309) and 3' homology (3R:7269313-7270955) arms, and gene targeting was performed as described (Koles et al. [2016], based on Chen et al. [2015]). Syt4-T-STEP flies were crossed to bam-Gal4;UAS-Rippase::PEST @attP2 flies to isolate germline ripouts of the TagRFPT cassette, leaving a C-terminal EGFP knock-in with the following linker (Syt4 sequence in lowercase, EGFP in italics, Precision protease site underlined): prrqiaewhklneSYALMKEY-VILSSSSGSSLEVLFGPGSGSGSMVSKGEELFTGV. The EGFP knockin strain was created by germline conversion of the T-STEP tag. All other fly stocks and sources are described in Table S1.

*Drosophila* larvae were cultured using standard media at controlled density at 25° for all experiments. Wandering third instar larvae were dissected in calcium-free HL3.1 saline (Feng et al., 2004) and fixed in HL3.1 containing 4% formaldehyde before antibody staining. Male larvae were used for all experiments, except for chloroquine treatment (Fig. S4, F and G) and *Vps35 rab11* genetic interaction experiments (Fig. 9, D and E), for which both male and female larvae were used. For chloroquine treatment, Formula 4-24 Instant *Drosophila* Medium (Carolina Biological Supply Company) was prepared at a 1:2 ratio with 0–8 mM chloroquine diluted in water and allowed to solidify at room temperature. Four male and four female larvae homozygous for Syt4-EGFP were added to each vial, and vials were incubated for up to 9 d at 25°C.

### Immunohistochemistry and imaging

For primary antibody information and concentrations, see Table S2. FluoTag-X4  $\alpha$ -GFP nanobodies (Nanotag Biotechnologies) were used to amplify EGFP signal for SIM imaging only; all other EGFP imaging reflects endogenous EGFP fluorescence. Primary and secondary incubations and washes were conducted in PBS with 0.5% Triton X-100, 2% (wt/vol) BSA, and 2% (vol/vol) normal goat serum, except Nrg staining, which was conducted with PBS with 0.2% Triton X-100 (no blocking agent).  $\alpha$ -HRP antibodies and secondary antibodies for imaging were conjugated to Dylight 488, Rhodamine Red-X, or Alexa 647 (Jackson ImmunoResearch) and were used at a concentration of 1:250 (Alexa 647) or 1:100 (Dylight 488 and Rhodamine Red-X). For LysoTracker staining, fillets were incubated with 1:100 LysoTracker Deep Red (Thermo Fisher Scientific; cat no. L12492) in PBS with no detergent for 10 min before fixation and mounting. Subsequent processing for immunohistochemistry was conducted as indicated above with the exception that no detergent was used. Samples were mounted in Vectashield (Vector Labs) for spinning-disk confocal and Airyscan imaging, and in Prolong Diamond (Thermo Fisher Scientific; cat no. P36965) for SIM.

NMJs on muscle 6/7 from segments A2 and A3 were selected for EV and colocalization analyses, and muscle 4 from the same segments was used for bouton counting. Spinning-disk confocal stacks were collected at room temperature, using Nikon Elements AR software, on a Nikon Ni-E upright microscope equipped with 60 $\times$  (NA, 1.4) and 100 $\times$  (NA, 1.45) oil immersion objectives, a Yokogawa CSU-W1 spinning-disk head, and an Andor iXon 897U EMCCD camera. Images for each independent experiment were acquired and are shown with identical settings for all conditions (except where indicated otherwise, and for all  $\alpha$ -HRP immunostaining, which was used to analyze morphology and not for intensity quantifications).

3D-SIM was performed at room temperature on a Nikon N-SIM E system (consisting of an inverted Eclipse Ti-E microscope, 100 $\times$  [NA, 1.45] oil-immersion objective, and a Hamamatsu OrcaFLASH4 sCMOS camera). Channel alignment was calculated for each imaging session using TetraSpeck beads (Invitrogen; cat no. T-7284). Images were collected at room temperature with a regimen of three grid orientations and five phases and were reconstructed using Nikon Elements software, using a theoretical, ideal optical transfer function generated by the software.

Airyscan microscopy was conducted at room temperature on a Zeiss 880 laser scanning microscope equipped with a Fast Airyscan detector, and operated in super resolution acquisition mode, using a 63 $\times$  NA 1.4 objective.

### Image analysis and statistics

3D analyses of presynaptic and postsynaptic EV cargo at NMJs were conducted using Velocity 6.0 software (Perkin Elmer). Manual thresholding of the  $\alpha$ -HRP signal was used to define presynaptic volume (HRP-positive objects >7  $\mu\text{m}^3$ , with holes filled) and postsynaptic volume (a dilation of 3  $\mu\text{m}$  around the presynaptic volume). The signal to be measured (see Table S3) was manually thresholded to distinguish postsynaptic puncta from background, and sum intensity measurements were made from EV cargo-positive objects intersecting with either presynaptic or postsynaptic volumes as defined above. All intensity values were then normalized to the presynaptic volume. Puncta number and volume were measured in presynaptic volumes that were thresholded and defined as above.

Analysis of APP-EGFP in axons and motor neuron cell bodies was conducted using ImageJ. Axon intensity measurements were conducted from maximum intensity projections (MaxIPs); HRP was used as a threshold to select a region of axon. APP intensity in motor neuron cell bodies was measured from a middle slice through each cell body.

Co-localization between APP and Rab11 was performed in Velocity. As above, the  $\alpha$ -HRP channel was used as a mask to highlight the presynaptic area. For quantitative analysis of SIM images, the following unbiased criteria were applied to select images with sufficiently high-quality staining and signal:noise ratio, and that were adequately free of reconstruction artifacts. Both channels required a presynaptic coefficient of variation (CoV) >0.1, and ratio of presynaptic APP CoV:postsynaptic APP CoV of >1.5. A threshold was set to identify all APP or Rab11-positive volumes in the HRP area, and the fraction of the sum

intensity of APP signal that coincided with Rab11 signal was calculated and vice versa.

### EM of larval NMJs

Wandering third instar larvae (three animals per condition) were dissected and fixed in 2.5% glutaraldehyde and 2% paraformaldehyde in 1% sodium cacodylate buffer overnight at 4°C. Samples were postfixed in 1% osmium tetroxide and 1.5% potassium ferrocyanide for 1 h, then 1% aqueous uranyl acetate for 1 h. Stepwise dehydration was conducted for 10 min each in 50%, 70%, and 90% ethanol, followed by 2 × 10 min in 100% ethanol. Samples were transferred to 100% propylene oxide for 1 h and then left overnight in a 1:1 mixture of propylene oxide and 812 TAAB Epon Resin (TAAB Laboratories Equipment Ltd.). Samples were then transferred to fresh epon, flat-embedded, polymerized at 60°C for 72 h, and remounted for sectioning. 70-μm-thin sections were cut on a Leica UC6 Ultramicrotome (Leica Microsystems), collected onto copper grids coated with formvar and carbon, and then poststained with lead citrate (Venable and Coggeshall, 1965). Grids were imaged using a FEI Morgagni transmission electron microscope (FEI) operating at 80 kV and equipped with a 1k × 1k charge coupled device camera (Gatan), or on a CM12 transmission electron microscope operating at 120 keV and equipped with LaB6 electron source and a Gatan Ultrascan 2k × 2k charge coupled device camera.

EM image analysis was performed on blinded images using FIJI. For quantification of endosomes and MVBs, endosomes were defined as presynaptic unilamellar compartments >100 nm at their longest axis. MVBs were defined as endosomes that contained one or more 50–100-nm intraluminal vesicles. Extracellular vesicles were measured as objects that were between 50 and 100 nm in diameter, within 1 μm of the neuron, and apparently free-floating (no contiguity with the SSR membrane). Numbers of endosomes, MVBs, and EVs were normalized to the area of the bouton.

### Statistical methods

All statistical measurements were performed in GraphPad Prism 6 (see Table S3). Comparisons were made separately for presynaptic and postsynaptic datasets, due to differences between these compartments for intensity, signal-to-noise ratio, and variance. Datasets were tested for normality, and statistical significance was tested using unpaired two-tailed Student's *t* tests or Mann–Whitney tests (if number of conditions was two) or ANOVA followed by Tukey's tests or Kruskal–Wallis followed by Dunn's test (if number of conditions was greater than two). Statistical significance is indicated as \*, *P* < 0.05; \*\*, *P* < 0.01; \*\*\*, *P* < 0.001.

### Online supplemental material

Fig. S1 shows that presynaptic APP and Appl localize to NMJ EVs. Fig. S2 shows neuronal retromer and APP trafficking. Fig. S3 depicts the characterization of Nrg as an EV cargo. Fig. S4 shows that lysosome dysfunction does not cause retromer-dependent EV cargo sorting defects. Fig. S5 depicts endosome distribution in *Vps26* and *Snx1*, *Snx6* mutants. Table S1 lists fly

strains. Table S2 lists antibodies and reagents. Table S3 provides genotypes and statistics by dataset.

### Acknowledgments

We thank the Bloomington *Drosophila* Stock Center (National Institutes of Health P40OD018537), the Developmental Studies Hybridoma Bank created by the National Institute of Child Health and Human Development of the National Institutes of Health, Konrad Bassler (University of Zurich, Zurich, Switzerland), Vivian Budnik (University of Massachusetts Medical School, Worcester, MA), Pete Cullen (University of Bristol, Bristol, UK), Xinhua Lin (Cincinnati Children's Hospital Medical Center, Cincinnati, OH), Kalpana White (Brandeis University, Waltham, MA), and Philip Copenhaver (Oregon Health and Science University, Portland, OR) for strains and reagents; and Crystal Yu, Troy Zhao, Agnieszka Collins, and the Brandeis EM Facility for technical assistance.

This work was supported by National Institute of Neurological Disorders and Stroke grants DP2 NS082127 and R01 NS103967 to A.A. Rodal, T32 GM007122 to R.B. Walsh, T32 NS007292 to E.C. Dresselhaus, T32 MH019929 to A.L. Scalera, and F32 NS110123 to C.R. Blanchette, and the Brandeis National Science Foundation Materials Research Science and Engineering Center, Bioinspired Soft Materials (NSF-DMR 2011846).

The authors declare no competing financial interests.

Author contributions: R.B. Walsh, A.N. Becalska, M.J. Zunitch, and A.A. Rodal designed the study and experiments. R.B. Walsh, E.C. Dresselhaus, A.N. Becalska, C.R. Blanchette, M.J. Zunitch, A.L. Scalera, J. Apiki, T. Lemos, S.M. Lee, S. Wang, B. Isaac, A. Yeh, and A.A. Rodal conducted the experiments and performed analyses. K. Koles generated critical reagents. R.B. Walsh and A.A. Rodal wrote the manuscript.

Submitted: 5 December 2020

Revised: 15 March 2021

Accepted: 29 April 2021

### References

- Akbergenova, Y., and J.T. Littleton. 2017. Pathogenic Huntington Alters BMP Signaling and Synaptic Growth through Local Disruptions of Endosomal Compartments. *J. Neurosci.* 37:3425–3439. <https://doi.org/10.1523/JNEUROSCI.2752-16.2017>
- Arbo, B.D., L.R. Cechinel, R.P. Palazzo, and I.R. Siqueira. 2020. Endosomal dysfunction impacts extracellular vesicle release: Central role in Aβ pathology. *Ageing Res. Rev.* 58:101006. <https://doi.org/10.1016/j.arr.2019.101006>
- Arighi, C.N., L.M. Hartnell, R.C. Aguilar, C.R. Haft, and J.S. Bonifacino. 2004. Role of the mammalian retromer in sorting of the cation-independent mannose 6-phosphate receptor. *J. Cell Biol.* 165:123–133. <https://doi.org/10.1083/jcb.200312055>
- Ashley, J., B. Cordy, D. Lucia, L.G. Fradkin, V. Budnik, and T. Thomson. 2018. Retrovirus-like Gag Protein Arc1 Binds RNA and Traffics across Synaptic Boutons. *Cell.* 172:262–274.e11. <https://doi.org/10.1016/j.cell.2017.12.022>
- Assaker, G., D. Ramel, S.K. Wculek, M. González-Gaitán, and G. Emery. 2010. Spatial restriction of receptor tyrosine kinase activity through a polarized endocytic cycle controls border cell migration. *Proc. Natl. Acad. Sci. USA.* 107:22558–22563. <https://doi.org/10.1073/pnas.1010795108>
- Baietti, M.F., Z. Zhang, E. Mortier, A. Melchior, G. Degeest, A. Geeraerts, Y. Ivarsson, F. Depoortere, C. Coomans, E. Vermeiren, et al. 2012.

- Syndecan-syntenin-ALIX regulates the biogenesis of exosomes. *Nat. Cell Biol.* 14:677–685. <https://doi.org/10.1038/ncb2502>
- Beckett, K., S. Monier, L. Palmer, C. Alexandre, H. Green, E. Bonneil, G. Raposo, P. Thibault, R. Le Borgne, and J.P. Vincent. 2013. *Drosophila* S2 cells secrete wingless on exosome-like vesicles but the wingless gradient forms independently of exosomes. *Traffic*. 14:82–96. <https://doi.org/10.1111/tra.12016>
- Bécot, A., C. Volgers, and G. van Niel. 2020. Transmissible Endosomal Intoxication: A Balance between Exosomes and Lysosomes at the Basis of Intercellular Amyloid Propagation. *Biomedicines*. 8:272. <https://doi.org/10.3390/biomedicines8080272>
- Belyaeva, E.S., M.G. Aizenzon, V.F. Semeshin, I.I. Kiss, K. Koczka, E.M. Baritcheva, T.D. Gorelova, and I.F. Zhimulev. 1980. Cytogenetic analysis of the 2B3-4--2B11 region of the X-chromosome of *Drosophila melanogaster*. I. Cytology of the region and mutant complementation groups. *Chromosoma*. 81:281–306. <https://doi.org/10.1007/BF00285954>
- Berman, D.E., D. Ringe, G.A. Petsko, and S.A. Small. 2015. The use of pharmacological retromer chaperones in Alzheimer's disease and other endosomal-related disorders. *Neurotherapeutics*. 12:12–18. <https://doi.org/10.1007/s13311-014-0321-y>
- Bhalla, A., C.P. Vetanovetz, E. Morel, Z. Chamoun, G. Di Paolo, and S.A. Small. 2012. The location and trafficking routes of the neuronal retromer and its role in amyloid precursor protein transport. *Neurobiol. Dis.* 47:126–134. <https://doi.org/10.1016/j.nbd.2012.03.030>
- Brodin, L., and O. Shupliakov. 2018. Retromer in Synaptic Function and Pathology. *Front. Synaptic Neurosci.* 10:37. <https://doi.org/10.3389/fnsyn.2018.00037>
- Budnik, V., Y.H. Koh, B. Guan, B. Hartmann, C. Hough, D. Woods, and M. Gorczyca. 1996. Regulation of synapse structure and function by the *Drosophila* tumor suppressor gene *dlg*. *Neuron*. 17:627–640. [https://doi.org/10.1016/S0896-6273\(00\)80196-8](https://doi.org/10.1016/S0896-6273(00)80196-8)
- Buggia-Prévot, V., C.G. Fernandez, S. Riordan, K.S. Vetrivel, J. Roseman, J. Waters, V.P. Bindokas, R. Vassar, and G. Thinakaran. 2014. Axonal BACE1 dynamics and targeting in hippocampal neurons: a role for Rab11 GTPase. *Mol. Neurodegener.* 9:1. <https://doi.org/10.1186/1750-1326-9-1>
- Cassar, M., and D. Kretzschmar. 2016. Analysis of Amyloid Precursor Protein Function in *Drosophila melanogaster*. *Front. Mol. Neurosci.* 9:61. <https://doi.org/10.3389/fnmol.2016.00061>
- Chen, H.M., Y. Huang, B.D. Pfeiffer, X. Yao, and T. Lee. 2015. An enhanced gene targeting toolkit for *Drosophila*: Golic+. *Genetics*. 199:683–694. <https://doi.org/10.1534/genetics.114.173716>
- Chen, K.E., M.D. Healy, and B.M. Collins. 2019. Towards a molecular understanding of endosomal trafficking by Retromer and Retriever. *Traffic*. 20:465–478. <https://doi.org/10.1111/tra.12649>
- Corrigan, L., S. Redhai, A. Leiblich, S.J. Fan, S.M. Perera, R. Patel, C. Gandy, S.M. Wainwright, J.F. Morris, F. Hamdy, et al. 2014. BMP-regulated exosomes from *Drosophila* male reproductive glands reprogram female behavior. *J. Cell Biol.* 206:671–688. <https://doi.org/10.1083/jcb.201401072>
- Cui, Y., J.M. Carosi, Z. Yang, N. Ariotti, M.C. Kerr, R.G. Parton, T.J. Sargeant, and R.D. Teasdale. 2019. Retromer has a selective function in cargo sorting via endosome transport carriers. *J. Cell Biol.* 218:615–631. <https://doi.org/10.1083/jcb.201806153>
- D'Souza, R.S., R. Semus, E.A. Billings, C.B. Meyer, K. Conger, and J.E. Casanova. 2014. Rab4 orchestrates a small GTPase cascade for recruitment of adaptor proteins to early endosomes. *Curr. Biol.* 24:1187–1198. <https://doi.org/10.1016/j.cub.2014.04.003>
- Daniels, R.W., M.V. Gelfand, C.A. Collins, and A. DiAntonio. 2008. Visualizing glutamatergic cell bodies and synapses in *Drosophila* larval and adult CNS. *J. Comp. Neurol.* 508:131–152. <https://doi.org/10.1002/cne.21670>
- Derivery, E., E. Helfer, V. Henriot, and A. Gautreau. 2012. Actin polymerization controls the organization of WASH domains at the surface of endosomes. *PLoS One*. 7:e39774. <https://doi.org/10.1371/journal.pone.0039774>
- Dermaut, B., K.K. Norga, A. Kania, P. Verstreken, H. Pan, Y. Zhou, P. Callaerts, and H.J. Bellen. 2005. Aberrant lysosomal carbohydrate storage accompanies endocytic defects and neurodegeneration in *Drosophila* benchwarmer. *J. Cell Biol.* 170:127–139. <https://doi.org/10.1083/jcb.200412001>
- Deshpande, M., Z. Feiger, A.K. Shilton, C.C. Luo, E. Silverman, and A.A. Rodal. 2016. Role of BMP receptor traffic in synaptic growth defects in an ALS model. *Mol. Biol. Cell*. 27:2898–2910. <https://doi.org/10.1091/mbc.E16-07-0519>
- Dollar, G., E. Struckhoff, J. Michaud, and R.S. Cohen. 2002. Rab11 polarization of the *Drosophila* oocyte: a novel link between membrane trafficking, microtubule organization, and oskar mRNA localization and translation. *Development*. 129:517–526. <https://doi.org/10.1242/dev.129.2.517>
- Dunst, S., T. Kazimiers, F. von Zadow, H. Jambor, A. Sagner, B. Brankatschk, A. Mahmoud, S. Spann, P. Tomancak, S. Eaton, and M. Brankatschk. 2015. Endogenously tagged rab proteins: a resource to study membrane trafficking in *Drosophila*. *Dev. Cell*. 33:351–365. <https://doi.org/10.1016/j.devcel.2015.03.022>
- Eisenberg, M., K. Gathy, T. Vincent, and J. Rawls. 1990. Molecular cloning of the UMP synthase gene rudimentary-like from *Drosophila melanogaster*. *Mol. Gen. Genet.* 222:1–8. <https://doi.org/10.1007/BF00283015>
- Eitan, E., C. Suire, S. Zhang, and M.P. Mattson. 2016. Impact of lysosome status on extracellular vesicle content and release. *Ageing Res. Rev.* 32:65–74. <https://doi.org/10.1016/j.arr.2016.05.001>
- Emery, G., A. Hutterer, D. Berdnik, B. Mayer, F. Wirtz-Peitz, M.G. Gaitan, and J.A. Knoblich. 2005. Asymmetric Rab 11 endosomes regulate delta recycling and specify cell fate in the *Drosophila* nervous system. *Cell*. 122:763–773. <https://doi.org/10.1016/j.cell.2005.08.017>
- Enneking, E.M., S.R. Kudumala, E. Moreno, R. Stephan, J. Boerner, T.A. Godenschwege, and J. Pielage. 2013. Transsynaptic coordination of synaptic growth, function, and stability by the Ll-type CAM Neuroglian. *PLoS Biol.* 11:e1001537. <https://doi.org/10.1371/journal.pbio.1001537>
- Entchev, E.V., A. Schwabedissen, and M. González-Gaitán. 2000. Gradient formation of the TGF-beta homolog Dpp. *Cell*. 103:981–992. [https://doi.org/10.1016/S0092-8674\(00\)00200-2](https://doi.org/10.1016/S0092-8674(00)00200-2)
- Escudero, C.A., O.M. Lazo, C. Galleguillos, J.I. Parraguez, M.A. Lopez-Verrilli, C. Cabeza, L. Leon, U. Saeed, C. Retamal, A. Gonzalez, et al. 2014. The p75 neurotrophin receptor evades the endolysosomal route in neuronal cells, favouring multivesicular bodies specialised for exosomal release. *J. Cell Sci.* 127:1966–1979. <https://doi.org/10.1242/jcs.141754>
- Fabrowski, P., A.S. Necakov, S. Mumbauer, E. Loeser, A. Reversi, S. Streichan, J.A. Briggs, and S. De Renzis. 2013. Tubular endocytosis drives remodelling of the apical surface during epithelial morphogenesis in *Drosophila*. *Nat. Commun.* 4:2244. <https://doi.org/10.1038/ncomms3244>
- Fan, S.J., B. Kroeger, P.P. Marie, E.M. Bridges, J.D. Mason, K. McCormick, C.E. Zois, H. Sheldon, N. Khalid Alham, E. Johnson, et al. 2020. Glutamine deprivation alters the origin and function of cancer cell exosomes. *EMBO J.* 39:e103009. <https://doi.org/10.15252/embj.2019103009>
- Feng, Y., A. Ueda, and C.F. Wu. 2004. A modified minimal hemolymph-like solution, HL3.1, for physiological recordings at the neuromuscular junctions of normal and mutant *Drosophila* larvae. *J. Neurogenet.* 18:377–402. <https://doi.org/10.1080/01677060490894522>
- Ferguson, S.M. 2018. Axonal transport and maturation of lysosomes. *Curr. Opin. Neurobiol.* 51:45–51. <https://doi.org/10.1016/j.conb.2018.02.020>
- Fernandes, A.C., V. Uytterhoeven, S. Kuenen, Y.C. Wang, J.R. Slabbaert, J. Swerts, J. Kaspricz, S. Aerts, and P. Verstreken. 2014. Reduced synaptic vesicle protein degradation at lysosomes curbs TBCLD24/sky-induced neurodegeneration. *J. Cell Biol.* 207:453–462. <https://doi.org/10.1083/jcb.201406026>
- Fjorback, A.W., M. Seaman, C. Gustafsen, A. Mehmedbasic, S. Gokool, C. Wu, D. Militz, V. Schmidt, P. Madsen, J.R. Nyengaard, et al. 2012. Retromer binds the FANSHY sorting motif in SorLA to regulate amyloid precursor protein sorting and processing. *J. Neurosci.* 32:1467–1480. <https://doi.org/10.1523/JNEUROSCI.2272-11.2012>
- Follett, J., S.J. Norwood, N.A. Hamilton, M. Mohan, O. Kovtun, S. Tay, Y. Zhe, S.A. Wood, G.D. Mellick, P.A. Silburn, et al. 2014. The Vps35 D620N mutation linked to Parkinson's disease disrupts the cargo sorting function of retromer. *Traffic*. 15:230–244. <https://doi.org/10.1111/tra.12136>
- French, K.C., M.A. Antonyak, and R.A. Cerione. 2017. Extracellular vesicle docking at the cellular port: Extracellular vesicle binding and uptake. *Semin. Cell Dev. Biol.* 67:48–55. <https://doi.org/10.1016/j.semcdb.2017.01.002>
- Fuentes-Medel, Y., M.A. Logan, J. Ashley, B. Ataman, V. Budnik, and M.R. Freeman. 2009. Glia and muscle sculpt neuromuscular arbors by engulfing destabilized synaptic boutons and shed presynaptic debris. *PLoS Biol.* 7:e1000184. <https://doi.org/10.1371/journal.pbio.1000184>
- Gonzalez-Noriega, A., J.H. Grubb, V. Talkad, and W.S. Sly. 1980. Chloroquine inhibits lysosomal enzyme pinocytosis and enhances lysosomal enzyme secretion by impairing receptor recycling. *J. Cell Biol.* 85:839–852. <https://doi.org/10.1083/jcb.85.3.839>
- Gross, J.C., V. Chaudhary, K. Bartscherer, and M. Boutros. 2012. Active Wnt proteins are secreted on exosomes. *Nat. Cell Biol.* 14:1036–1045. <https://doi.org/10.1038/ncb2574>
- Harbour, M.E., S.Y. Breusegem, R. Antrobus, C. Freeman, E. Reid, and M.N. Seaman. 2010. The cargo-selective retromer complex is a recruiting

- hub for protein complexes that regulate endosomal tubule dynamics. *J. Cell Sci.* 123:3703–3717. <https://doi.org/10.1242/jcs.071472>
- Hazelrigg, T., R. Levis, and G.M. Rubin. 1984. Transformation of white locus DNA in drosophila: dosage compensation, zeste interaction, and position effects. *Cell.* 36:469–481. [https://doi.org/10.1016/0092-8674\(84\)90240-X](https://doi.org/10.1016/0092-8674(84)90240-X)
- Holm, M.M., J. Kaiser, and M.E. Schwab. 2018. Extracellular Vesicles: Multimodal Envoys in Neural Maintenance and Repair. *Trends Neurosci.* 41: 360–372. <https://doi.org/10.1016/j.tins.2018.03.006>
- Hortsch, M., A.J. Bieber, N.H. Patel, and C.S. Goodman. 1990. Differential splicing generates a nervous system-specific form of *Drosophila* neuroglian. *Neuron.* 4:697–709. [https://doi.org/10.1016/0896-6273\(90\)90196-M](https://doi.org/10.1016/0896-6273(90)90196-M)
- Huntwork, S., and J.T. Littleton. 2007. A complexin fusion clamp regulates spontaneous neurotransmitter release and synaptic growth. *Nat. Neurosci.* 10:1235–1237. <https://doi.org/10.1038/nn1980>
- Inoshita, T., T. Arano, Y. Hosaka, H. Meng, Y. Umezaki, S. Kosugi, T. Morimoto, M. Koike, H.Y. Chang, Y. Imai, and N. Hattori. 2017. Vps35 in cooperation with LRRK2 regulates synaptic vesicle endocytosis through the endosomal pathway in *Drosophila*. *Hum. Mol. Genet.* 26:2933–2948. <https://doi.org/10.1093/hmg/ddx179>
- Jia, D., T.S. Gomez, D.D. Billadeau, and M.K. Rosen. 2012. Multiple repeat elements within the FAM21 tail link the WASH actin regulatory complex to the retromer. *Mol. Biol. Cell.* 23:2352–2361. <https://doi.org/10.1091/mbc.e11-12-1059>
- Jimenez-Orgaz, A., A. Kvainickas, H. Nägele, J. Denner, S. Eimer, J. Dengjel, and F. Steinberg. 2018. Control of RAB7 activity and localization through the retromer-TBC1D5 complex enables RAB7-dependent mitophagy. *EMBO J.* 37:235–254. <https://doi.org/10.15252/embj.201797128>
- Juhász, G., J.H. Hill, Y. Yan, M. Sass, E.H. Baehrecke, J.M. Backer, and T.P. Neufeld. 2008. The class III PI(3)K Vps34 promotes autophagy and endocytosis but not TOR signaling in *Drosophila*. *J. Cell Biol.* 181:655–666. <https://doi.org/10.1093/jcb.200712051>
- Kanmert, D., A. Cantlon, C.R. Muratore, M. Jin, T.T. O'Malley, G. Lee, T.L. Young-Pearse, D.J. Selkoe, and D.M. Walsh. 2015. C-Terminally Truncated Forms of Tau, But Not Full-Length Tau or Its C-Terminal Fragments, Are Released from Neurons Independently of Cell Death. *J. Neurosci.* 35:10851–10865. <https://doi.org/10.1523/JNEUROSCI.0387-15.2015>
- Koles, K., J. Nunnari, C. Korkut, R. Barria, C. Brewer, Y. Li, J. Leszyk, B. Zhang, and V. Budnik. 2012. Mechanism of evenness interrupted (Evi)-exosome release at synaptic boutons. *J. Biol. Chem.* 287:16820–16834. <https://doi.org/10.1074/jbc.M112.342667>
- Koles, K., A.R. Yeh, and A.A. Rodal. 2016. Tissue-specific tagging of endogenous loci in *Drosophila melanogaster*. *Biol. Open.* 5:83–89. <https://doi.org/10.1242/bio.016089>
- Koles, K., E.M. Messelaar, Z. Feiger, C.J. Yu, C.A. Frank, and A.A. Rodal. 2015. The EHD protein Past1 controls postsynaptic membrane elaboration and synaptic function. *Mol. Biol. Cell.* 26:3275–3288. <https://doi.org/10.1091/mbc.e15-02-0093>
- Korkut, C., B. Ataman, P. Ramachandran, J. Ashley, R. Barria, N. Gherbesi, and V. Budnik. 2009. Trans-synaptic transmission of vesicular Wnt signals through Evi/Wntless. *Cell.* 139:393–404. <https://doi.org/10.1016/j.cell.2009.07.051>
- Korkut, C., Y. Li, K. Koles, C. Brewer, J. Ashley, M. Yoshihara, and V. Budnik. 2013. Regulation of postsynaptic retrograde signaling by presynaptic exosome release. *Neuron.* 77:1039–1046. <https://doi.org/10.1016/j.neuron.2013.01.013>
- Korolchuk, V.I., M.M. Schütz, C. Gómez-Llorente, J. Rocha, N.R. Lansu, S.M. Collins, Y.P. Wairkar, I.M. Robinson, and C.J. O'Kane. 2007. *Drosophila* Vps35 function is necessary for normal endocytic trafficking and actin cytoskeleton organisation. *J. Cell Sci.* 120:4367–4376. <https://doi.org/10.1242/jcs.012336>
- Kvainickas, A., H. Nägele, W. Qi, L. Dokládal, A. Jimenez-Orgaz, L. Stehl, D. Gangurde, Q. Zhao, Z. Hu, J. Dengjel, et al. 2019. Retromer and TBC1D5 maintain late endosomal RAB7 domains to enable amino acid-induced mTORC1 signaling. *J. Cell Biol.* 218:3019–3038. <https://doi.org/10.1083/jcb.201812110>
- Laulagnier, K., C. Javalet, F.J. Hemming, M. Chivet, G. Lachenal, B. Blot, C. Chatellard, and R. Sadoul. 2018. Amyloid precursor protein products concentrate in a subset of exosomes specifically endocytosed by neurons. *Cell. Mol. Life Sci.* 75:757–773. <https://doi.org/10.1007/s00018-017-2664-0>
- Lauwers, E., Y.C. Wang, R. Gallardo, R. Van der Kant, E. Michiels, J. Swerts, P. Baatsen, S.S. Zaiter, S.R. McAlpine, N.V. Gounko, et al. 2018. Hsp90 Mediates Membrane Deformation and Exosome Release. *Mol. Cell.* 71: 689–702.e9. <https://doi.org/10.1016/j.molcel.2018.07.016>
- Lazarov, O., M. Lee, D.A. Peterson, and S.S. Sisodia. 2002. Evidence that synaptically released beta-amyloid accumulates as extracellular deposits in the hippocampus of transgenic mice. *J. Neurosci.* 22:9785–9793. <https://doi.org/10.1523/JNEUROSCI.22-22-09785.2002>
- Li, J., T. Kanekiyo, M. Shinohara, Y. Zhang, M.J. LaDu, H. Xu, and G. Bu. 2012. Differential regulation of amyloid- $\beta$  endocytic trafficking and lysosomal degradation by apolipoprotein E isoforms. *J. Biol. Chem.* 287: 44593–44601. <https://doi.org/10.1074/jbc.M112.420224>
- Li, J.G., J. Chiu, and D. Praticò. 2020. Full recovery of the Alzheimer's disease phenotype by gain of function of vacuolar protein sorting 35. *Mol. Psychiatry.* 25:2630–2640. <https://doi.org/10.1038/s41380-019-0364-x>
- Lin, D.M., and C.S. Goodman. 1994. Ectopic and increased expression of Fasciclin II alters motoneuron growth cone guidance. *Neuron.* 13: 507–523. [https://doi.org/10.1016/0896-6273\(94\)90022-1](https://doi.org/10.1016/0896-6273(94)90022-1)
- Linhart, R., S.A. Wong, J. Cao, M. Tran, A. Huynh, C. Ardrey, J.M. Park, C. Hsu, S. Taha, R. Peterson, et al. 2014. Vacuolar protein sorting 35 (Vps35) rescues locomotor deficits and shortened lifespan in *Drosophila* expressing a Parkinson's disease mutant of Leucine-Rich Repeat Kinase 2 (LRRK2). *Mol. Neurodegener.* 9:23. <https://doi.org/10.1186/1750-1326-9-23>
- Lundgren, J.L., S. Ahmed, B. Winblad, G.K. Gouras, L.O. Tjernberg, and S. Frykman. 2014. Activity-independent release of the amyloid  $\beta$ -peptide from rat brain nerve terminals. *Neurosci. Lett.* 566:125–130. <https://doi.org/10.1016/j.neulet.2014.02.050>
- Luo, L.Q., L.E. Martin-Morris, and K. White. 1990. Identification, secretion, and neural expression of APPL, a *Drosophila* protein similar to human amyloid protein precursor. *J. Neurosci.* 10:3849–3861. <https://doi.org/10.1523/JNEUROSCI.10-12-03849.1990>
- Luo, L., T. Tully, and K. White. 1992. Human amyloid precursor protein ameliorates behavioral deficit of flies deleted for App1 gene. *Neuron.* 9: 595–605. [https://doi.org/10.1016/0896-6273\(92\)90024-8](https://doi.org/10.1016/0896-6273(92)90024-8)
- Malik, B.R., V.K. Godena, and A.J. Whitworth. 2015. VPS35 pathogenic mutations confer no dominant toxicity but partial loss of function in *Drosophila* and genetically interact with parkin. *Hum. Mol. Genet.* 24: 6106–6117. <https://doi.org/10.1093/hmg/ddv322>
- Marie, P.P., S.-J. Fan, C.C. Mendes, S.M. Wainwright, A.L. Harris, D.C.I. Gøberdhan, and C. Wilson. 2020. Accessory ESCRT-III proteins selectively regulate Rab11-exosome biogenesis in *Drosophila* secondary cells. *bioRxiv*. (Preprint posted June 18, 2020) <https://doi.org/10.1101/2020.06.18.158725>
- Maruzs, T., P. Lőrincz, Z. Szatmári, S. Széplaki, Z. Sándor, Z. Lakatos, G. Puska, G. Juhász, and M. Sass. 2015. Retromer Ensures the Degradation of Autophagic Cargo by Maintaining Lysosome Function in *Drosophila*. *Traffic.* 16:1088–1107. <https://doi.org/10.1111/tra.12309>
- McGough, I.J., F. Steinberg, D. Jia, P.A. Barbuti, K.J. McMillan, K.J. Heesom, A.L. Whone, M.A. Caldwell, D.D. Billadeau, M.K. Rosen, and P.J. Cullen. 2014. Retromer binding to FAM21 and the WASH complex is perturbed by the Parkinson disease-linked VPS35(D620N) mutation. *Curr. Biol.* 24: 1670–1676. <https://doi.org/10.1016/j.cub.2014.06.024>
- Méresse, S., J.P. Gorvel, and P. Chavrier. 1995. The rab7 GTPase resides on a vesicular compartment connected to lysosomes. *J. Cell Sci.* 108: 3349–3358. <https://doi.org/10.1242/jcs.108.11.3349>
- Miranda, A.M., Z.M. Lasiecka, Y. Xu, J. Neufeld, S. Shahriar, S. Simoes, R.B. Chan, T.G. Oliveira, S.A. Small, and G. Di Paolo. 2018. Neuronal lysosomal dysfunction releases exosomes harboring APP C-terminal fragments and unique lipid signatures. *Nat. Commun.* 9:291. <https://doi.org/10.1038/s41467-017-02533-w>
- Miura, E., T. Hasegawa, M. Konno, M. Suzuki, N. Sugeno, N. Fujikake, S. Geisler, M. Tabuchi, R. Oshima, A. Kikuchi, et al. 2014. VPS35 dysfunction impairs lysosomal degradation of  $\alpha$ -synuclein and exacerbates neurotoxicity in a *Drosophila* model of Parkinson's disease. *Neurobiol. Dis.* 71:1–13. <https://doi.org/10.1016/j.nbd.2014.07.014>
- Muhammad, A., I. Flores, H. Zhang, R. Yu, A. Staniszewski, E. Planel, M. Herman, L. Ho, R. Kreber, L.S. Honig, et al. 2008. Retromer deficiency observed in Alzheimer's disease causes hippocampal dysfunction, neurodegeneration, and Abeta accumulation. *Proc. Natl. Acad. Sci. USA.* 105:7327–7332. <https://doi.org/10.1073/pnas.0802545105>
- Narayanan, R., H. Krämer, and M. Ramaswami. 2000. *Drosophila* endosomal proteins hook and deep orange regulate synapse size but not synaptic vesicle recycling. *J. Neurobiol.* 45:105–119. [https://doi.org/10.1002/1097-4695\(20001105\)45:2<105::AID-NEU5>3.0.CO;2-X](https://doi.org/10.1002/1097-4695(20001105)45:2<105::AID-NEU5>3.0.CO;2-X)
- Naslavsky, N., and S. Caplan. 2018. The enigmatic endosome - sorting the ins and outs of endocytic trafficking. *J. Cell Sci.* 131:jcs216499. <https://doi.org/10.1242/jcs.216499>

- Neuman, S.D., E.L. Terry, J.E. Selegue, A.T. Cavanagh, and A. Bashirullah. 2021. Mistargeting of secretory cargo in retromer-deficient cells. *Dis. Model. Mech.* 14:dmm046417. <https://doi.org/10.1242/dmm.046417>
- Ni, J.Q., M. Markstein, R. Binari, B. Pfeiffer, L.P. Liu, C. Villalta, M. Booker, L. Perkins, and N. Perrimon. 2008. Vector and parameters for targeted transgenic RNA interference in *Drosophila melanogaster*. *Nat. Methods* 5: 49–51. <https://doi.org/10.1038/nmeth1146>
- Nielsen, M.S., C. Gustafsen, P. Madsen, J.R. Nyengaard, G. Hermey, O. Bakke, M. Mari, P. Schu, R. Pohlmann, A. Denness, and C.M. Petersen. 2007. Sorting by the cytoplasmic domain of the amyloid precursor protein binding receptor SorLA. *Mol. Cell. Biol.* 27:6842–6851. <https://doi.org/10.1128/MCB.00815-07>
- Norris, A., P. Tammineni, S. Wang, J. Gerdes, A. Murr, K.Y. Kwan, Q. Cai, and B.D. Grant. 2017. SNX-1 and RME-8 oppose the assembly of HGRS-1/ESCRT-0 degradative microdomains on endosomes. *Proc. Natl. Acad. Sci. USA* 114:E307–E316. <https://doi.org/10.1073/pnas.1612730114>
- Parks, A.L., K.R. Cook, M. Belvin, N.A. Dompe, R. Fawcett, K. Huppert, L.R. Tan, C.G. Winter, K.P. Bogart, J.E. Deal, et al. 2004. Systematic generation of high-resolution deletion coverage of the *Drosophila melanogaster* genome. *Nat. Genet.* 36:288–292. <https://doi.org/10.1038/ng1312>
- Port, F., M. Kuster, P. Herr, E. Furger, C. Bänziger, G. Hausmann, and K. Basler. 2008. Wingless secretion promotes and requires retromer-dependent cycling of Wntless. *Nat. Cell Biol.* 10:178–185. <https://doi.org/10.1038/ncb1687>
- Rink, J., E. Ghigo, Y. Kalaidzidis, and M. Zerial. 2005. Rab conversion as a mechanism of progression from early to late endosomes. *Cell* 122: 735–749. <https://doi.org/10.1016/j.cell.2005.06.043>
- Rojas, R., T. van Vlijmen, G.A. Mardones, Y. Prabhu, A.L. Rojas, S. Mohammed, A.J. Heck, G. Raposo, P. van der Sluijs, and J.S. Bonifacino. 2008. Regulation of retromer recruitment to endosomes by sequential action of Rab5 and Rab7. *J. Cell Biol.* 183:513–526. <https://doi.org/10.1083/jcb.200804048>
- Satoh, A.K., J.E. O'Tousa, K. Ozaki, and D.F. Ready. 2005. Rab11 mediates post-Golgi trafficking of rhodopsin to the photosensitive apical membrane of *Drosophila* photoreceptors. *Development* 132:1487–1497. <https://doi.org/10.1242/dev.01704>
- Savina, A., M. Vidal, and M.I. Colombo. 2002. The exosome pathway in K562 cells is regulated by Rab11. *J. Cell Sci.* 115:2505–2515. <https://doi.org/10.1242/jcs.115.12.2505>
- Seaman, M.N.J. 2021. The Retromer Complex: From Genesis to Revelations. *Trends Biochem. Sci.*:S0968-0004(20)30321-2. <https://doi.org/10.1016/j.tibs.2020.12.009>
- Seaman, M.N., J.M. McCaffery, and S.D. Emr. 1998. A membrane coat complex essential for endosome-to-Golgi retrograde transport in yeast. *J. Cell Biol.* 142:665–681. <https://doi.org/10.1083/jcb.142.3.665>
- Seaman, M.N., M.E. Harbour, D. Tattersall, E. Read, and N. Bright. 2009. Membrane recruitment of the cargo-selective retromer subcomplex is catalysed by the small GTPase Rab7 and inhibited by the Rab-GAP TBC1D5. *J. Cell Sci.* 122:2371–2382. <https://doi.org/10.1242/jcs.048686>
- Seaman, M.N., A. Gautreau, and D.D. Billadeau. 2013. Retromer-mediated endosomal protein sorting: all WASHed up! *Trends Cell Biol.* 23: 522–528. <https://doi.org/10.1016/j.tcb.2013.04.010>
- Seaman, M.N.J., A.S. Mukadam, and S.Y. Breusegem. 2018. Inhibition of TBC1D5 activates Rab7a and can enhance the function of the retromer cargo-selective complex. *J. Cell Sci.* 131:jcs217398. <https://doi.org/10.1242/jcs.217398>
- Shimizu, H., S. Kawamura, and K. Ozaki. 2003. An essential role of Rab5 in uniformity of synaptic vesicle size. *J. Cell Sci.* 116:3583–3590. <https://doi.org/10.1242/jcs.00676>
- Simonetti, B., C.M. Danson, K.J. Heesom, and P.J. Cullen. 2017. Sequence-dependent cargo recognition by SNX-BARs mediates retromer-independent transport of CI-MPR. *J. Cell Biol.* 216:3695–3712. <https://doi.org/10.1083/jcb.201703015>
- Simonetti, B., B. Paul, K. Chaudhari, S. Weeratunga, F. Steinberg, M. Gorla, K.J. Heesom, G.J. Bashaw, B.M. Collins, and P.J. Cullen. 2019. Molecular identification of a BAR domain-containing coat complex for endosomal recycling of transmembrane proteins. *Nat. Cell Biol.* 21:1219–1233. <https://doi.org/10.1038/s41556-019-0393-3>
- Small, S.A., K. Kent, A. Pierce, C. Leung, M.S. Kang, H. Okada, L. Honig, J.P. Vonsattel, and T.W. Kim. 2005. Model-guided microarray implicates the retromer complex in Alzheimer's disease. *Ann. Neurol.* 58:909–919. <https://doi.org/10.1002/ana.20667>
- Snow, P.M., N.H. Patel, A.L. Harrelson, and C.S. Goodman. 1987. Neural-specific carbohydrate moiety shared by many surface glycoproteins in *Drosophila* and grasshopper embryos. *J. Neurosci.* 7:4137–4144. <https://doi.org/10.1523/JNEUROSCI.07-12-04137.1987>
- Song, P., K. Trajkovic, T. Tsunemi, and D. Krainc. 2016. Parkin Modulates Endosomal Organization and Function of the Endo-Lysosomal Pathway. *J. Neurosci.* 36:2425–2437. <https://doi.org/10.1523/JNEUROSCI.2569-15.2016>
- Song, Z., Y. Xu, W. Deng, L. Zhang, H. Zhu, P. Yu, Y. Qu, W. Zhao, Y. Han, and C. Qin. 2020. Brain Derived Exosomes Are a Double-Edged Sword in Alzheimer's Disease. *Front. Mol. Neurosci.* 13:79. <https://doi.org/10.3389/fnmol.2020.00079>
- Steinberg, F., M. Gallon, M. Winfield, E.C. Thomas, A.J. Bell, K.J. Heesom, J.M. Tavaré, and P.J. Cullen. 2013. A global analysis of SNX27-retromer assembly and cargo specificity reveals a function in glucose and metal ion transport. *Nat. Cell Biol.* 15:461–471. <https://doi.org/10.1038/ncb2721>
- Stenmark, H., R.G. Parton, O. Steele-Mortimer, A. Lütcke, J. Gruenberg, and M. Zerial. 1994. Inhibition of rab5 GTPase activity stimulates membrane fusion in endocytosis. *EMBO J.* 13:1287–1296. <https://doi.org/10.1002/j.1460-2075.1994.tb06381.x>
- Strutt, H., P.F. Langton, N. Pearson, K.J. McMillan, D. Strutt, and P.J. Cullen. 2019. Retromer Controls Planar Polarity Protein Levels and Asymmetric Localization at Intercellular Junctions. *Curr. Biol.* 29:484–491.e6. <https://doi.org/10.1016/j.cub.2018.12.027>
- Sullivan, C.P., A.G. Jay, E.C. Stack, M. Pakaluk, E. Wadlinger, R.E. Fine, J.M. Wells, and P.J. Morin. 2011. Retromer disruption promotes amyloidogenic APP processing. *Neurobiol. Dis.* 43:338–345. <https://doi.org/10.1016/j.nbd.2011.04.002>
- Swanson, T.L., L.M. Knittel, T.M. Coate, S.M. Farley, M.A. Snyder, and P.F. Copenhaver. 2005. The insect homologue of the amyloid precursor protein interacts with the heterotrimeric G protein G $\alpha$  in an identified population of migratory neurons. *Dev. Biol.* 288:160–178. <https://doi.org/10.1016/j.ydbio.2005.09.029>
- Sweeney, S.T., and G.W. Davis. 2002. Unrestricted synaptic growth in spinster-a late endosomal protein implicated in TGF-beta-mediated synaptic growth regulation. *Neuron* 36:403–416. [https://doi.org/10.1016/S0896-6273\(02\)01014-0](https://doi.org/10.1016/S0896-6273(02)01014-0)
- Tan, J.Z.A., and P.A. Gleeson. 2019. The role of membrane trafficking in the processing of amyloid precursor protein and production of amyloid peptides in Alzheimer's disease. *Biochim. Biophys. Acta Biomembr.* 1861: 697–712. <https://doi.org/10.1016/j.bbmem.2018.11.013>
- Temkin, P., B. Lauffer, S. Jäger, P. Cimermancic, N.J. Krogan, and M. von Zastrow. 2011. SNX27 mediates retromer tubule entry and endosome-to-plasma membrane trafficking of signalling receptors. *Nat. Cell Biol.* 13:715–721. <https://doi.org/10.1038/ncb2252>
- Théry, C., K.W. Witwer, E. Aikawa, M.J. Alcaraz, J.D. Anderson, R. Andriantsitohaina, A. Antoniou, T. Arab, F. Archer, G.K. Atkin-Smith, et al. 2018. Minimal information for studies of extracellular vesicles 2018 (MISEV2018): a position statement of the International Society for Extracellular Vesicles and update of the MISEV2014 guidelines. *J. Extracell. Vesicles* 7:1535750. <https://doi.org/10.1080/20013078.2018.1535750>
- Toh, W.H., J.Z. Tan, K.L. Zulkefli, F.J. Houghton, and P.A. Gleeson. 2017. Amyloid precursor protein traffics from the Golgi directly to early endosomes in an Arl5b- and AP4-dependent pathway. *Traffic* 18:159–175. <https://doi.org/10.1111/tra.12465>
- Torroja, L., M. Packard, M. Gorczyca, K. White, and V. Budnik. 1999. The *Drosophila* beta-amyloid precursor protein homolog promotes synapse differentiation at the neuromuscular junction. *J. Neurosci.* 19:7793–7803. <https://doi.org/10.1523/JNEUROSCI.19-18-07793.1999>
- Udayar, V., V. Buggia-Prévot, R.L. Guerreiro, G. Siegel, N. Rambabu, A.L. Soohoo, M. Ponnusamy, B. Siegenthaler, J. Bali, M. Simons, et al. AEGS. 2013. A paired RNAi and RabGAP overexpression screen identifies Rab11 as a regulator of  $\beta$ -amyloid production. *Cell Rep.* 5:1536–1551. <https://doi.org/10.1016/j.celrep.2013.12.005>
- Ullrich, O., S. Reinsch, S. Urbé, M. Zerial, and R.G. Parton. 1996. Rab11 regulates recycling through the pericentriolar recycling endosome. *J. Cell Biol.* 135:913–924. <https://doi.org/10.1083/jcb.135.4.913>
- van Niel, G., D'Angelo, and G. Raposo. 2018. Shedding light on the cell biology of extracellular vesicles. *Nat. Rev. Mol. Cell Biol.* 19:213–228. <https://doi.org/10.1038/nrm.2017.125>
- Vardarajan, B.N., S.Y. Bruesegem, M.E. Harbour, R. Inzelberg, R. Friedland, P. St George-Hyslop, M.N. Seaman, and L.A. Farrer. 2012. Identification of Alzheimer disease-associated variants in genes that regulate retromer function. *Neurobiol. Aging* 33:2231.e15–2231.e30. <https://doi.org/10.1016/j.neurobiolaging.2012.04.020>
- Vazquez-Sanchez, S., S. Bobeldijk, M.P. Dekker, L. van Keimpema, and J.R.T. van Weering. 2018. VPS35 depletion does not impair presynaptic

- structure and function. *Sci. Rep.* 8:2996. <https://doi.org/10.1038/s41598-018-20448-4>
- Venable, J.H., and R. Coggeshall. 1965. A Simplified Lead Citrate Stain for Use in Electron Microscopy. *J. Cell Biol.* 25:407–408. <https://doi.org/10.1083/jcb.25.2.407>
- Vingtdeux, V., M. Hamdane, A. Loyens, P. Gelé, H. Drobeck, S. Bégard, M.C. Galas, A. Delacourte, J.C. Beauvillain, L. Buée, and N. Sergeant. 2007. Alkalinizing drugs induce accumulation of amyloid precursor protein by-products in luminal vesicles of multivesicular bodies. *J. Biol. Chem.* 282: 18197–18205. <https://doi.org/10.1074/jbc.M609475200>
- Wang, C.L., F.L. Tang, Y. Peng, C.Y. Shen, L. Mei, and W.C. Xiong. 2012a. VPS35 regulates developing mouse hippocampal neuronal morphogenesis by promoting retrograde trafficking of BACE1. *Biol. Open.* 1: 1248–1257. <https://doi.org/10.1242/bio.20122451>
- Wang, J.W., E.S. Beck, and B.D. McCabe. 2012b. A modular toolset for recombination transgenesis and neurogenetic analysis of *Drosophila*. *PLoS One.* 7:e42102. <https://doi.org/10.1371/journal.pone.0042102>
- Wang, S., K.L. Tan, M.A. Agosto, B. Xiong, S. Yamamoto, H. Sandoval, M. Jaiswal, V. Bayat, K. Zhang, W.L. Charng, et al. 2014. The retromer complex is required for rhodopsin recycling and its loss leads to photoreceptor degeneration. *PLoS Biol.* 12:e1001847. <https://doi.org/10.1371/journal.pbio.1001847>
- Wen, L., F.L. Tang, Y. Hong, S.W. Luo, C.L. Wang, W. He, C. Shen, J.U. Jung, F. Xiong, D.H. Lee, et al. 2011. VPS35 haploinsufficiency increases Alzheimer's disease neuropathology. *J. Cell Biol.* 195:765–779. <https://doi.org/10.1083/jcb.201105109>
- West, R.J., Y. Lu, B. Marie, F.B. Gao, and S.T. Sweeney. 2015. Rab8, POSH, and TAK1 regulate synaptic growth in a *Drosophila* model of frontotemporal dementia. *J. Cell Biol.* 208:931–947. <https://doi.org/10.1083/jcb.201404066>
- Wilcke, M., L. Johannes, T. Galli, V. Mayau, B. Goud, and J. Salamero. 2000. Rab11 regulates the compartmentalization of early endosomes required for efficient transport from early endosomes to the trans-golgi network. *J. Cell Biol.* 151:1207–1220. <https://doi.org/10.1083/jcb.151.6.1207>
- Winckler, B., V. Faundez, S. Maday, Q. Cai, C. Guimas Almeida, and H. Zhang. 2018. The Endolysosomal System and Proteostasis: From Development to Degeneration. *J. Neurosci.* 38:9364–9374. <https://doi.org/10.1523/JNEUROSCI.1665-18.2018>
- Ye, H., S.A. Ojelade, D. Li-Kroeger, Z. Zuo, L. Wang, Y. Li, J.Y. Gu, U. Tepass, A.A. Rodal, H.J. Bellen, and J.M. Shulman. 2020. Retromer subunit, VPS29, regulates synaptic transmission and is required for endolysosomal function in the aging brain. *eLife.* 9:e51977. <https://doi.org/10.7554/eLife.51977>
- Yong, X., L. Zhao, W. Deng, H. Sun, X. Zhou, L. Mao, W. Hu, X. Shen, Q. Sun, D.D. Billadeau, et al. 2020. Mechanism of cargo recognition by retromer-linked SNX-BAR proteins. *PLoS Biol.* 18:e3000631. <https://doi.org/10.1371/journal.pbio.3000631>
- Yu, Y., D.C. Jans, B. Winblad, L.O. Tjernberg, and S. Schedin-Weiss. 2018. Neuronal A $\beta$ 42 is enriched in small vesicles at the presynaptic side of synapses. *Life Sci. Alliance.* 1:e201800028. <https://doi.org/10.26508/lsa.201800028>
- Zavodszky, E., M.N. Seaman, K. Moreau, M. Jimenez-Sanchez, S.Y. Breusegem, M.E. Harbour, and D.C. Rubinsztein. 2014. Mutation in VPS35 associated with Parkinson's disease impairs WASH complex association and inhibits autophagy. *Nat. Commun.* 5:3828. <https://doi.org/10.1038/ncomms4828>
- Zhang, J., K.L. Schulze, P.R. Hiesinger, K. Suyama, S. Wang, M. Fish, M. Acar, R.A. Hoskins, H.J. Bellen, and M.P. Scott. 2007. Thirty-one flavors of *Drosophila* rab proteins. *Genetics.* 176:1307–1322. <https://doi.org/10.1534/genetics.106.066761>
- Zhang, P., Y. Wu, T.Y. Belenkaya, and X. Lin. 2011. SNX3 controls Wingless/Wnt secretion through regulating retromer-dependent recycling of Wntless. *Cell Res.* 21:1677–1690. <https://doi.org/10.1038/cr.2011.167>

## Supplemental material

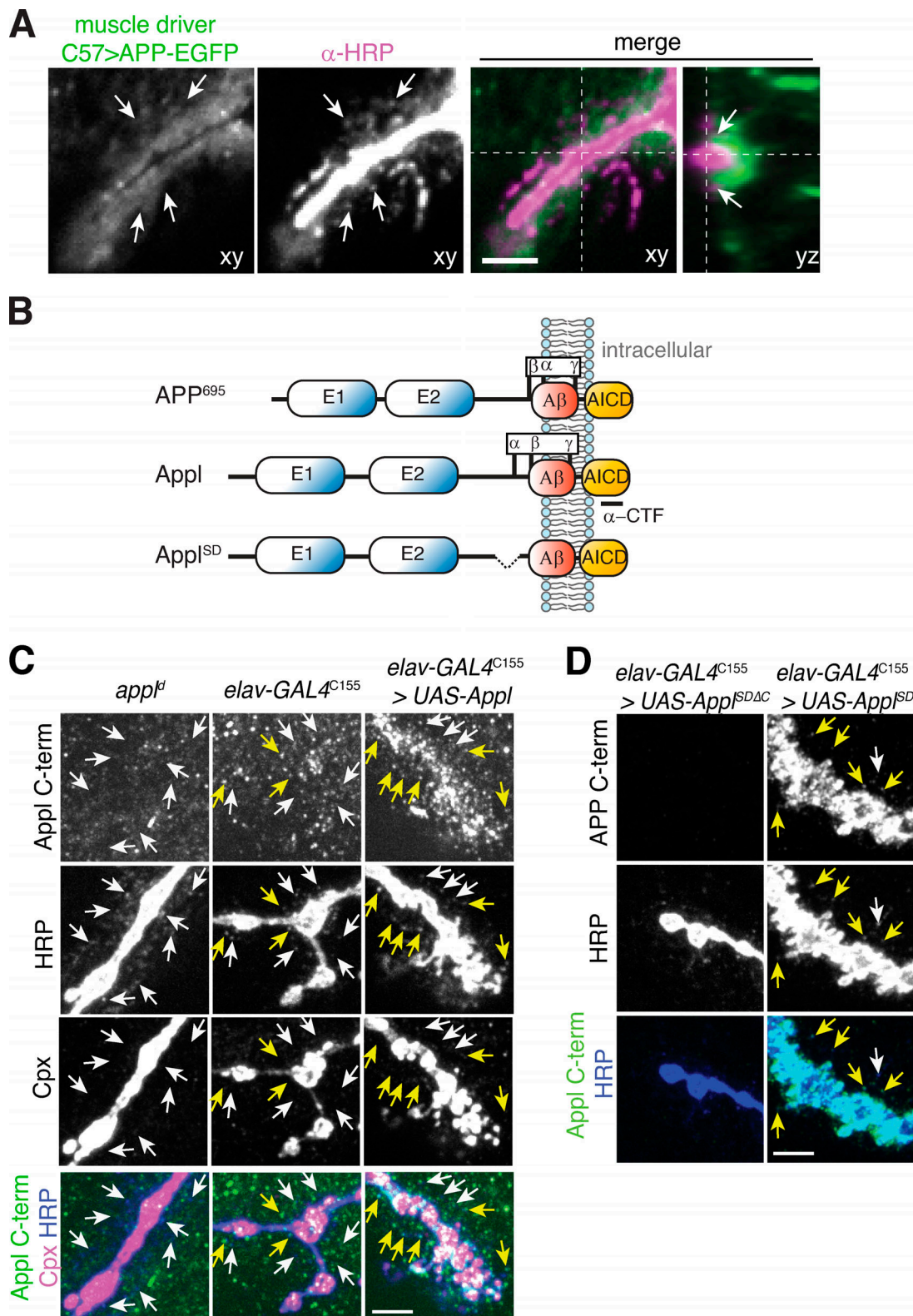


Figure S1. **Presynaptic APP and Appl localize to NMJ EVs.** (A) Confocal images of NMJs from animals expressing muscle-driven ( $GAL4^{C57}$ ) UAS-APP-EGFP, stained with  $\alpha$ -HRP. Arrows indicate presynaptically derived HRP-positive puncta that do not colocalize with muscle-derived APP. (B) Schematic of domain organization and mutants in *Drosophila* Appl. AICD, APP intracellular domain; E, extracellular; CTF, C-terminal fragment. (C) MaxIPs showing EV localization of *Drosophila* Appl. Yellow arrows indicate puncta that are positive for both Appl and  $\alpha$ -HRP. White arrows indicate puncta that are solely  $\alpha$ -HRP-positive. Cpx (presynaptic marker) is absent from Appl and  $\alpha$ -HRP puncta. (D) MaxIP showing EV localization of *Drosophila* Appl<sup>SD</sup>, and absence of  $\alpha$ -Appl C-terminal (C-term) antibody immunostaining for Appl<sup>SDΔC</sup>. Yellow arrows indicate puncta that are positive for both Appl and  $\alpha$ -HRP. Note that image display settings for  $\alpha$ -Appl are different between C and D in order to visualize Appl<sup>SD</sup>, which expresses at high levels. All scale bars are 5  $\mu$ m. Associated with Fig. 1.

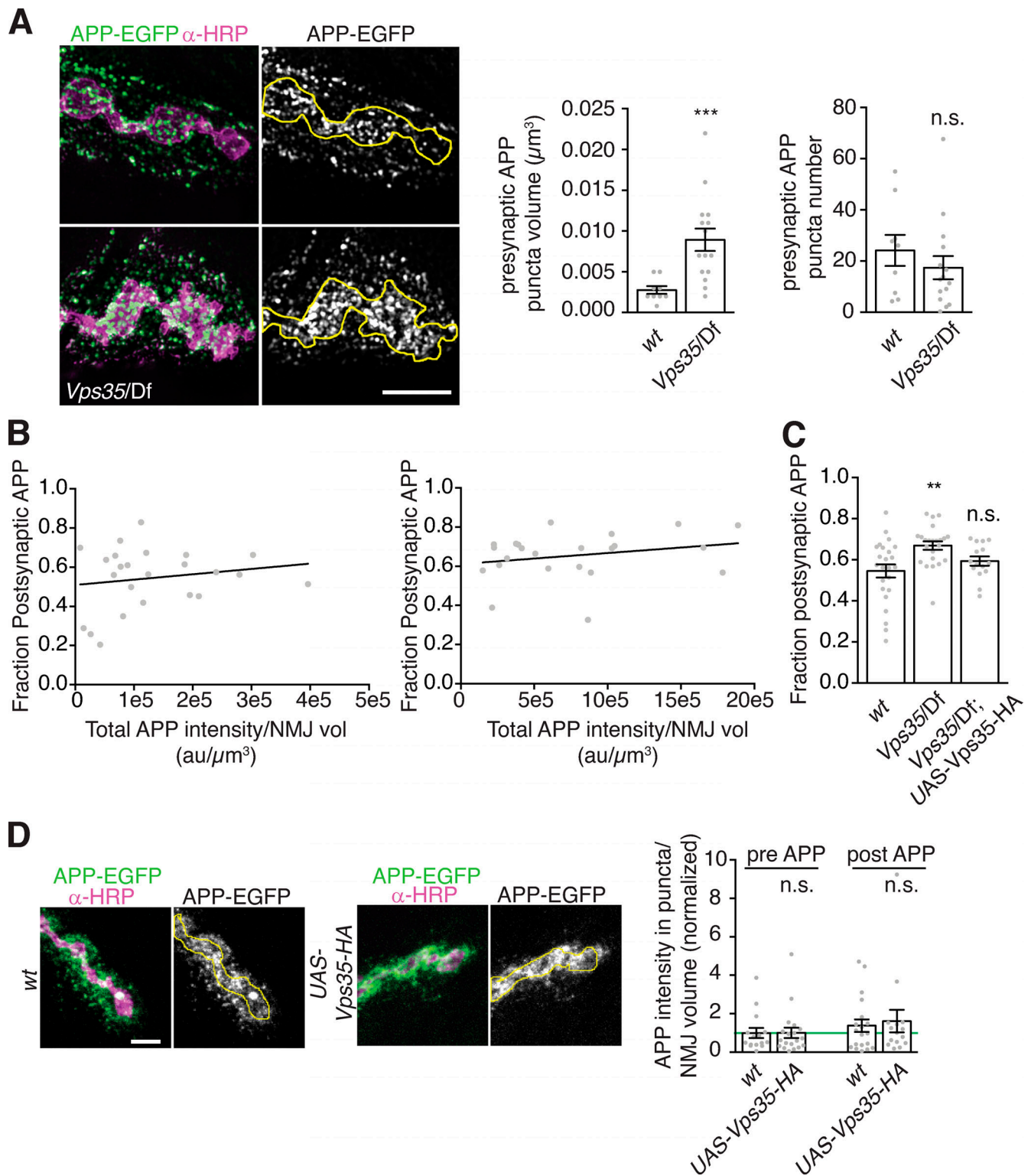


Figure S2. **Neuronal retromer and APP trafficking.** (A) APP-containing compartments are larger in *Vps35* mutants. MaxIPs and quantification of representative SIM images of NMJs expressing APP-EGFP in the indicated genotypes. Yellow line indicates presynaptic region; scale bar is 2  $\mu\text{m}$ . (B) Dataset from Fig. 2, B and C; the fraction of postsynaptic APP-EGFP versus total APP-EGFP at *Vps35* mutant NMJs is not strongly correlated. (C) Dataset from Fig. 2, B and C; the fraction of APP-EGFP that is postsynaptic slightly increases in *Vps35* NMJs. (D) Controls for *Vps35*-HA rescue. Neuronal UAS-*Vps35*-HA expression does not affect levels of APP-EGFP in a wild-type background. Scale bar is 5  $\mu\text{m}$ . Measurements were normalized to presynaptic mean of control (green line). Yellow lines indicate presynaptic region; bar graphs show mean  $\pm$  SEM; dots show all data points representing individual NMJs. See Table S3 for detailed genotypes and statistical tests. Associated with Fig. 2. \*\*,  $P < 0.01$ ; \*\*\*,  $P < 0.001$ .

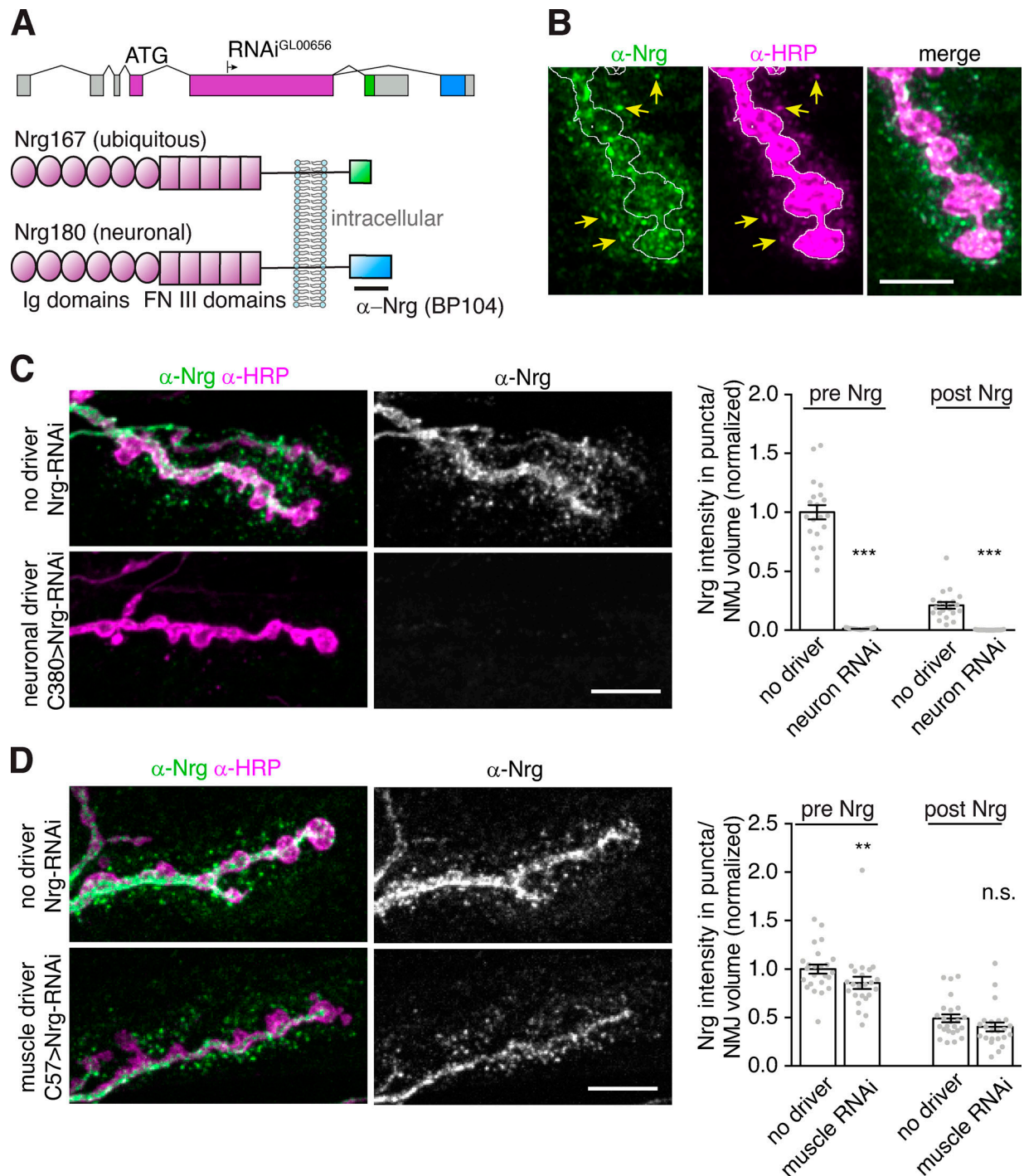


Figure S3. **Characterization of Nrg as an EV cargo.** Nrg is a cell adhesion molecule for which an excellent monoclonal antibody exists. Previous reports indicate an EV-like localization for Nrg (Enneking et al., 2013), which we further validate here to enable its use as a convenient EV marker. **(A)** Schematic of domain organization, RNAi target, and antibody binding site for *Drosophila* Nrg. FN III, fibronectin type III. **(B)** MaxIPs of Airyscan confocal stacks showing EV localization of Nrg. Yellow arrows indicate puncta that are positive for both  $\alpha$ -Nrg and  $\alpha$ -HRP signals, suggesting that postsynaptic Nrg is in EVs surrounded by neuronally derived membrane; white line outlines the  $\alpha$ -HRP-labeled presynaptic terminal. Scale bar is 5  $\mu$ m. **(C)** Presynaptic knockdown of Nrg depletes presynaptic and postsynaptic signal, indicating that all NMJ Nrg is derived from the neuron and released in EVs. **(D)** Postsynaptic knockdown of Nrg causes a mild presynaptic reduction, but no change to postsynaptic signal (as previously observed; Enneking et al., 2013). MaxIPs of representative SDCM images (left) and quantification (right), normalized to mean intensity of wild-type control. Scale bars in C and D are 10  $\mu$ m. All bar graphs show mean  $\pm$  SEM; dots show all data points representing individual NMJs. See Table S3 for detailed genotypes and statistical tests. Associated with Fig. 3. \*\*,  $P < 0.01$ ; \*\*\*,  $P < 0.001$ .

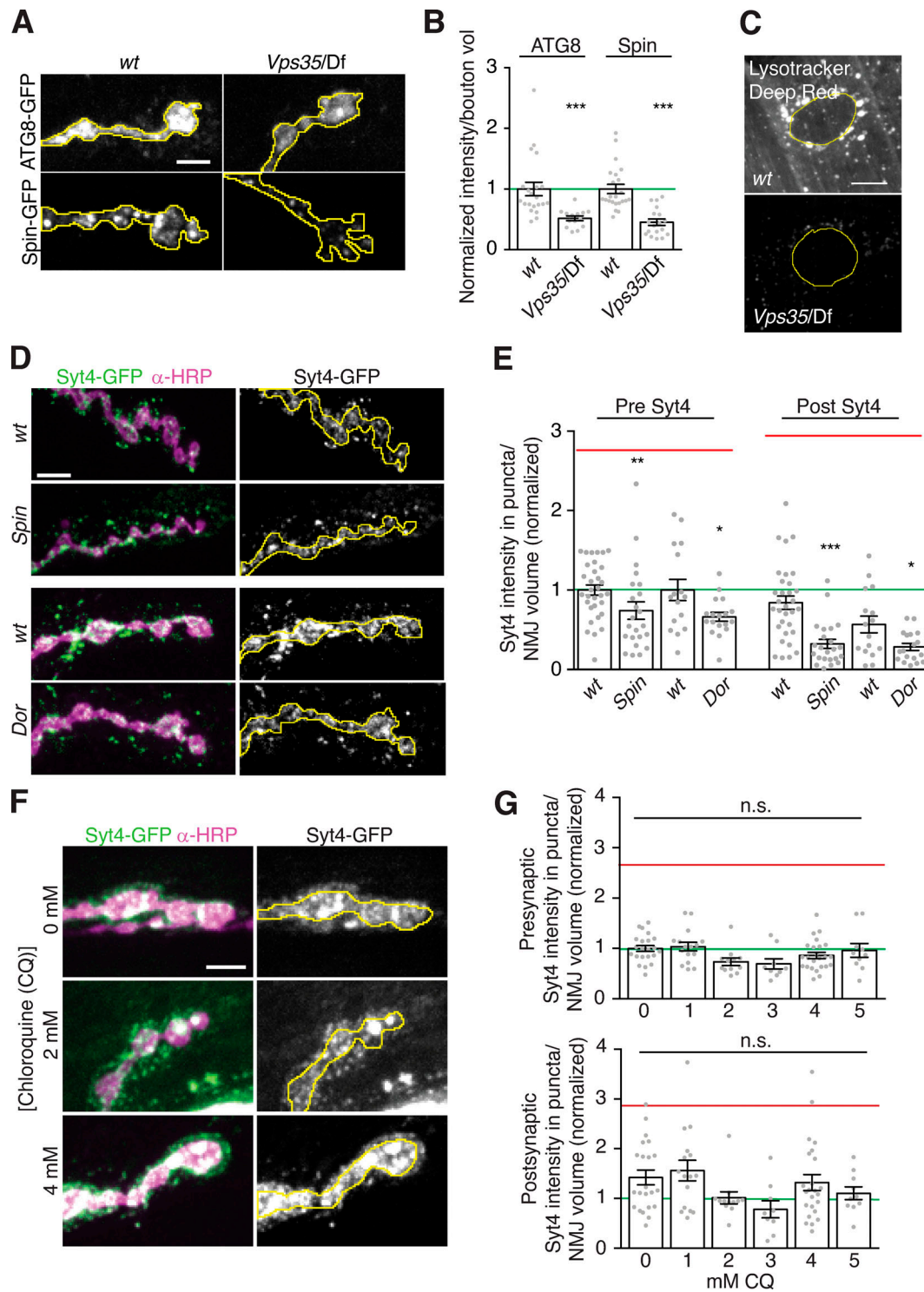


Figure S4. **Lysosome dysfunction does not cause retromer-dependent EV cargo sorting defects. (A–C)** Retromer loss does not cause accumulation of lysosome-like compartments. **(A)** MaxIPs of NMJs from larvae expressing neuronally driven Spin-GFP or ATG8-GFP. Yellow line outlines  $\alpha$ -HRP-labeled presynaptic terminal. **(B)** Quantification of A, normalized to mean intensity of wild-type control (green line). **(C)** MaxIPs of NMJs and the muscle perinuclear region labeled with LysoTracker Deep Red. Muscles exhibit a decrease in LysoTracker intensity indicating a reduction in acidified lysosomal compartments. Yellow line outlines muscle nucleus. **(D and E)** Mutants that disrupt lysosome function do not exhibit EV cargo accumulation or increased postsynaptic EV cargo. **(D)** MaxIPs of NMJs from larvae expressing endogenously tagged Syt4-EGFP. Yellow line outlines  $\alpha$ -HRP-labeled presynaptic terminal. **(E)** Quantification of D. **(F and G)** Pharmacological inhibition of lysosome function does not affect EV cargo levels. **(F)** MaxIPs of NMJs from larvae expressing endogenously tagged Syt4-EGFP and treated with the indicated concentration of chloroquine (CQ). Yellow line outlines  $\alpha$ -HRP-labeled presynaptic terminal. **(G)** Quantification of F. All conditions normalized to control. Red line indicates mean Syt4-EGFP levels in *Vps35* mutants from Fig. 3. Yellow lines indicate presynaptic regions; scale bars are 5  $\mu$ m. Bar graphs show mean  $\pm$  SEM; dots show all data points representing individual NMJs. See Table S3 for detailed genotypes and statistical tests. \*,  $P < 0.05$ ; \*\*,  $P < 0.01$ ; \*\*\*,  $P < 0.001$ .

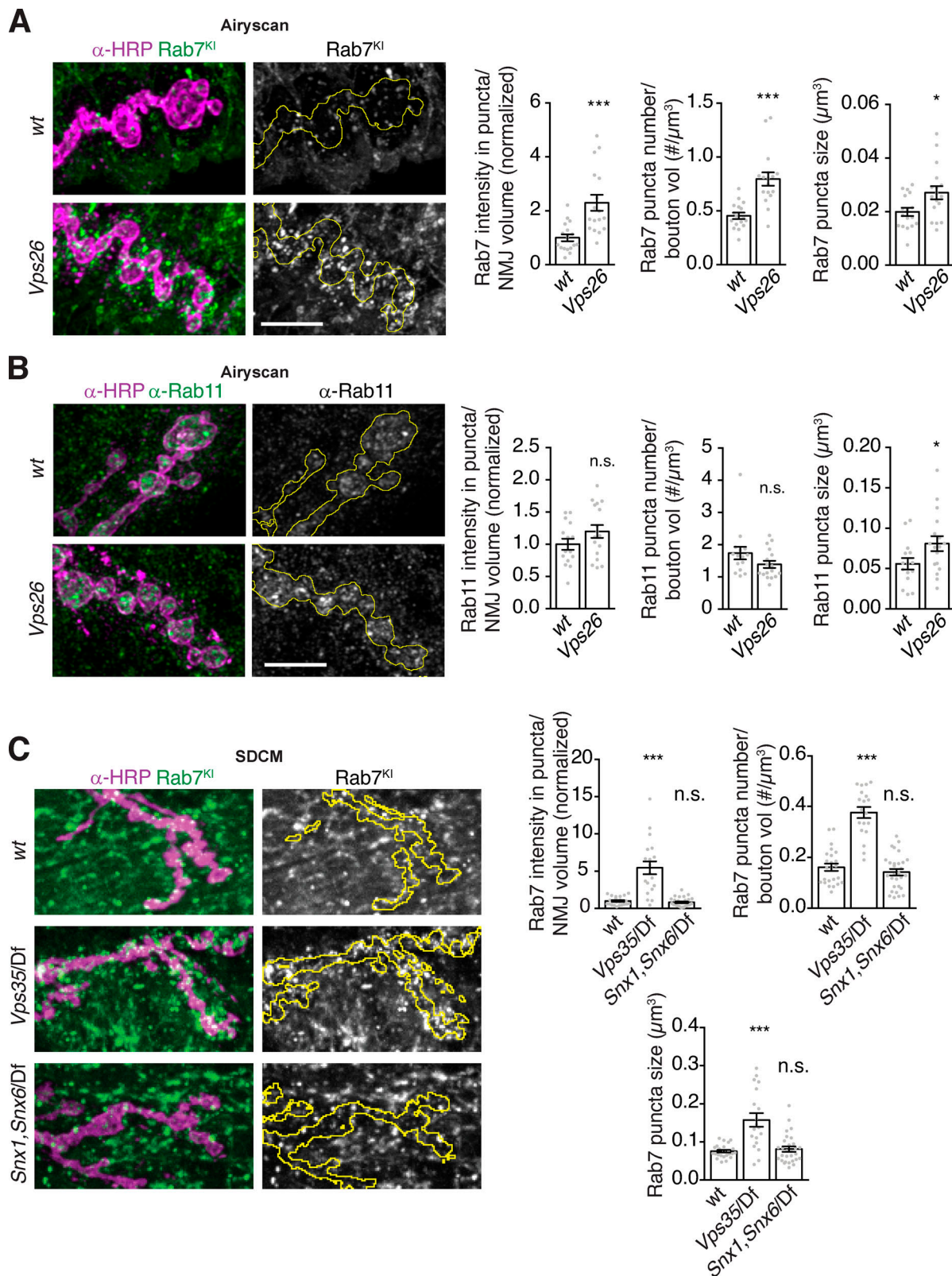


Figure S5. **Endosome distribution in *Vps26* and *Snx1, Snx6* mutants.** (A) Airyscan microscopy MaxIPs and quantification of presynaptic (endogenously tagged) YFP-Rab7 intensity, and endosome number and size in control or *Vps26* mutant backgrounds. (B) Airyscan microscopy MaxIPs and quantification of presynaptic  $\alpha$ -Rab11 intensity, and endosome number and size in control or *Vps26* mutant backgrounds. (C) SDCM MaxIPs and quantification of presynaptic (endogenously tagged) YFP-Rab7 intensity, and endosome number and size in control, *Vps35*, or *Snx1, Snx6* mutant backgrounds. Yellow lines indicate pre-synaptic regions; scale bars are 5  $\mu\text{m}$ . Bar graphs show mean  $\pm$  SEM; dots show all data points representing individual NMJs. See Table S3 for genotypes and statistical tests. Associated with Fig. 7. \*,  $P < 0.05$ ; \*\*\*,  $P < 0.001$ .

Tables S1, S2, and S3 are provided as separate files online. Table S1 lists fly strains. Table S2 lists antibodies. Table S3 provides genotypes and statistics by dataset.